Title page (Original Research Article)

Characterisation of RNA editing and gene therapy with a compact CRISPR-Cas13 in the retina

Satheesh Kumar[1,2,3], Yi-Wen Hsiao[1], Vickie H Y Wong[4], Deborah Aubin[5,6], Jiang-Hui Wang[1], Leszek Lisowski[7,8,9], Elizabeth P Rakoczy[10], Fan Li[11], Luis Alarcon-Martinez[1,2], Anai Gonzalez-Cordero[5,6], Bang V Bui[4], Guei-Sheung Liu[1,2,3*]

[1]Centre for Eye Research Australia, Royal Victorian Eye and Ear Hospital, East Melbourne, VIC, Australia.

[2]Ophthalmology, Department of Surgery, University of Melbourne, East Melbourne, VIC, Australia.

[3]Menzies Institute for Medical Research, University of Tasmania, Hobart, TAS, Australia.

[4]Department of Optometry and Vision Sciences, University of Melbourne, Parkville, VIC, Australia.

[5]School of Medical Sciences, Faculty of Medicine and Health, The University of Sydney, Camperdown, NSW, Australia.

[6]Stem Cell Medicine Group, Children's Medical Research Institute, Westmead, NSW, Australia.

[7]Translational Vectorology Research Unit, Children's Medical Research Institute, Faculty of Medicine and Health, The University of Sydney, Westmead, NSW, Australia.

[8]Military Institute of Medicine, Laboratory of Molecular Oncology and Innovative Therapies, Warsaw, Poland.

[9]Australian Genome Therapeutics Centre, Children's Medical Research Institute and Sydney Children's Hospitals Network, Westmead, NSW, Australia.

[10]Centre for Ophthalmology and Visual Sciences, University of Western Australia, Perth, WA, Australia.

27 [11]Eye Center, Zhongshan City People's Hospital, Zhongshan, Guangdong Province, China.

28 *Correspondence and requests for materials should be addressed to

29 Dr Guei-Sheung Liu (rickliu0817@gmail.com). Centre for Eye Research Australia. Address:
30 Level 7, 32 Gisborne Street, East Melbourne, VIC 3002, Australia. Tel: +61399298360.

31

32 Key words: RNA silencing, CRISPR-Cas13, angiogenesis, ocular neovascularization, diabetic
33 retinopathy, gene therapy, retinal organoids

34

35

36

Abstract

CRISPR-Cas13 nucleases are programmable RNA-targeting effectors that can silence gene expression in a reversible manner. Recent iterations of Cas13 nucleases are compact for adeno-associated virus (AAV) delivery to achieve strong and persistent expression in various organs in a safe manner. Here, we report significant transcriptomic signatures of Cas13bt3 expression and show all-in-one AAV gene therapy with Cas13bt3 can effectively silence *VEGFA* in human retinal organoids and humanised mouse models. Specifically, human embryonic stem cells (hESC)-derived retinal pigment epithelium cells show high expression of Cas13bt3 from virus delivery corresponding to significant reduction of *VEGFA* mRNA. We further show that intravitreal delivery of Cas13bt3 can transduce mouse retinal cells efficiently, reaching the photoreceptors for specific knockdown of human *VEGFA* in the trVEGF029 (Kimba) mouse. Our results reveal important considerations for assessing Cas13 activity and establishing Cas13bt3 as a potential anti-VEGF agent that can achieve long-term control of VEGFA for treatment of diabetic retinopathy and wet age-related macular degeneration.

52 **Introduction**

53 The emergence of Clustered Regularly Interspaced Short Palindromic Repeats (CRISPR) and
54 CRISPR-associated (Cas) enzymes, known as CRISPR-Cas, has fuelled several gene editing
55 efforts for novel therapeutics in the past decade(*1*). Developed by repurposing the bacterial
56 immune defence against phage viruses, CRISPR-Cas harnesses the ability to induce targeted
57 changes to DNA or RNA sequences. Among CRISPR-Cas proteins, CRISPR-Cas13 is of
58 particular interest for its exclusive specificity for RNA. Targeting RNA is especially attractive
59 as it enables control of gene expression without perturbing the genome and introducing
60 permanent changes and is therefore an emerging avenue for therapeutic development(*2*).

61 Eleven variants of CRISPR-Cas13 have been described to date(*3*). Among them, Cas13d
62 (commonly referred to as CasRx) described in 2018 garnered special attention for its compact
63 size of 930aa, making it the first Cas13 enzyme amenable to adeno-associated virus (AAV)
64 delivery. Studies investigating the development of RNA-targeting therapeutics have widely
65 used CasRx to demonstrate preclinical efficacy against disorders affecting vision, hearing and
66 brain function(*4-7*), however significant unintended editing have been reported, hampering its
67 clinical progress(*8, 9*), and the exact specificity profile of CasRx remains contested(*10*). More
68 recently, hypercompact Cas13bt3 (also reported as Cas13X) enzymes were described, ranging
69 even smaller at 775aa(*11, 12*). The newfound enzyme has been reported to possess high
70 specificity, and its small size enables additional applications such as RNA base editing using a
71 single AAV(*13-15*). The therapeutic potential of Cas13bt3 is yet to be demonstrated, however
72 initial *in vitro* studies show promising efficiency and safety(*13, 16*).

73 As a leading cause of blindness in the elderly population affecting 200 million people globally,
74 ocular neovascularisation refers to a group of conditions characterised by the abnormal growth
75 of leaky blood vessels in the eye. Vascular endothelial growth factor (VEGF) has been
76 described as a key mediator of this process, and the overexpression of *VEGFA* underlies
77 pathological angiogenesis and neovascularisation in common ocular diseases like diabetic
78 retinopathy (DR) and neovascular age-related macular degeneration (nAMD). Regular
79 (monthly/ bimonthly) administration of anti-VEGF drugs is the approved front-line treatment
80 modality for these patients(*17*). Delivered through intravitreal injections, frequent
81 administration of anti-VEGF drugs poses a significant clinical burden on healthcare institutions

82 and patients due to risk of infection, patient anxiety, clinic capacity and availability of trained
83 healthcare personnel among others(*18*).

84 We have previously described a potential alternative therapy to current anti-VEGF injections
85 using an all-in-one AAV CRISPR-CasRx gene therapy for the treatment of ocular
86 neovascularisation. This approach was validated *in vitro* in HEK293FT and MIO-M1 cells,
87 demonstrating more than 90% and 50% *VEGFA* mRNA knockdown, respectively(*19*). Here,
88 we utilize the novel Cas13bt3 to demonstrate potent *VEGFA* knockdown *in vitro* in human cell
89 lines, in 3D human embryonic stem cells (hESC)-derived retinal organoids and *in vivo* in
90 transgenic humanised mouse retinas. Promisingly, our results show significant knockdown of
91 *VEGFA* mRNA in human cell lines without impact on predicted off-target genes. Single cell
92 RNA sequencing (scRNA-seq) was used to characterise Cas13bt3-mediated *VEGFA* mRNA
93 knockdown at single cell resolution in human retinal organoids identifying, for the first time,
94 the overall transcriptomic impact and cell-specific activity of the enzyme. Lastly, *in vivo* gene
95 therapy showed robust *VEGFA* mRNA silencing in mouse models of proliferative diabetic
96 retinopathy along with control of neovascularisation symptoms. These findings support the
97 development of Cas13-mediated ocular gene therapy establishing the clinical potential of
98 Cas13bt3 and offering an alternative treatment to current anti-VEGF treatments.

99

100 **Results**

101 ***CRISPR-Cas13bt3 can knock down VEGFA mRNA in mammalian cells with minimal***
102 ***unintended targeting activity***

103 We used our previously described single guide RNAs (sgRNA) targeting Exon 4 of *VEGFA*
104 (*19*), to develop our new Cas13bt3 constructs and assess RNA cutting efficiency as well as
105 collateral and off target cleavages (**Figure 1A-D**). Collateral activity is the trans-cleavage by
106 Cas13 enzymes of adjacent mRNA transcripts as the result of an activated nuclease domain
107 (**Figure 1B**). Off-target activity, on the other hand, is the targeting of other non-target mRNA
108 transcripts due to unspecific binding of the sgRNA (**Figure 1C**).

109 We sought to compare and validate efficiency of the new Cas13bt3 enzyme by testing RNA
110 cutting against two previously established RNA-targeting methods, RNA interference (short
111 hairpin RNA, shRNA) and CasRx (a variant of Cas13d). These are widely used for therapeutic

112 and diagnostic applications. The final all-in-one AAV plasmids carrying either *VEGFA*-
113 targeting shRNA or precursor single guide RNA (sgRNA hereafter) with either CasRx or
114 Cas13bt3 (**Figure 1E**) were transfected into HEK293FT cells. Here, to further enhance the
115 expression of Cas13bt3 we incorporated the stronger cytomegalovirus (CMV) promoter instead
116 of the previously used elongation factor 1α short (EFS) promoter.

117 Significant *VEGFA* mRNA knockdown was observed from all three RNA-targeting methods,
118 with up to 70% shRNA *VEGFA* mRNA knockdown ($P < 0.001$), while CasRx and Cas13bt3
119 achieved up to 90% knockdown ($P < 0.0001$) compared to vector controls (AAV plasmid
120 carrying a fluorescent marker) (**Figure 1F**, n = 4 independent experiments). Next, we sought
121 to determine if the reduction in mRNA would also lead to a decrease in protein levels.
122 Interestingly, ELISAs for VEGFA revealed that only the Cas13bt3 treatment led to significant
123 reduction of VEGFA protein in the cell supernatant (**Figure 1G**, $P< 0.05$; n = 4 independent
124 experiments). As both Cas13 variants proved potent in silencing *VEGFA* mRNA in HEK293FT
125 cells, we next transfected immortalised human retinal pigment epithelium cells (ARPE19 cell
126 line) with the *VEGFA*-targeting CasRx and Cas13bt3 plasmids and again observed up to 90%
127 knockdown ($P < 0.05$, n = 3 independent experiments) with Cas13bt3 against vector controls
128 (**Figure S1**), suggesting that Cas13bt3 is a promising candidate for RNA silencing of retinal
129 cells.

130 To further understand transcriptome-wide effects, we performed bulk RNA sequencing (RNA-
131 seq) on HEK293FT cells transfected with shRNA, CasRx and Cas13bt3. RNA-seq was also
132 performed on cells treated with either control, Cas13bt3 only, Cas13bt3NT and
133 Cas13bt3VEGFA constructs to identify collateral and off-target activity of Cas13.
134 Differentially expressed genes (DEGs) were similar for all treated groups, shRNA, CasRx and
135 Cas13bt3 (**Figure S2A-C**), indicating that collateral activity from the new Cas13bt3 is
136 comparable to previously established RNA-targeting methods. Interestingly, the non-targeting
137 (NT) sgRNA group exhibited the highest number of DEGs, a finding that corresponds with
138 recent studies (**Figures 1G, H and S2A-D**) (*16, 20*). Volcano plots of Cas13bt3 samples
139 against control demonstrated and confirmed a significant downregulation of *VEGFA* mRNA
140 only on cells that received the VEGFA targeting treatment (**Figure 1I).**

141 We identified potential off-target genes through NCBI BLAST of our VEGFA sgRNA
142 sequence and studied the expression levels of the top 10 candidate off-target genes (**Figure**

143 **S3A**). None of the off-target genes were significantly downregulated, indicating lack of off-
144 target activity from Cas13bt3 (**Figure 1J**), as was the case for shRNA and CasRx (**Figure**
145 **S2F**).

146 To further examine the varying DEG levels between the NT and targeting sgRNAs, we
147 identified the top significantly enriched gene ontology (GO) terms for the Cas13bt3-NT
148 sgRNA and Cas13bt3-VEGFA sgRNA groups. Top 5 significant GO terms for the Cas13bt3-
149 NT sgRNA group were all positive enrichments and specifically showed upregulation of RNA
150 binding processes, such as "*pre-mRNA binding*" and "*mRNA 3' UTR binding*", possibly
151 explaining the elevated levels of DEGs in this group. On the other hand, with a VEGFA
152 sgRNA, the top 5 GO terms were all negative enrichments and particularly showed
153 downregulation of "*platelet-derived growth factor (PDGF) binding*" and "*PDGF receptor*
154 *binding*", both angiogenesis promoting factors (**Figure 1K**). A recent study showed CasRx to
155 have intrinsic targets that affected essential processes like RNA metabolism and mitotic cell
156 cycle (*20*) and opined that this could underlie the lethality seen upon CasRx expression in a
157 mouse model (*21*). Here, we found laminin-related processes (e.g., "*laminin binding*", "*laminin*
158 *complex*") were strongly downregulated across all groups (Cas13bt3 only, Cas13bt3-NT
159 sgRNA and Cas13bt3-VEGFA sgRNA) suggesting intrinsic targets could exist for Cas13bt3
160 as well (**Data S1**).

161 While Cas13bt3 may undergo activation after maturation of a NT sgRNA; without adequate
162 homologous pairing, the catalytic pocket cannot be formed for efficient nuclease activity (*22*).
163 On the other hand, with a targeting gRNA, Cas13bt3 would be activated to form the Cas13bt3-
164 gRNA-target complex for targeted knockdown. Our results suggest that with a NT sgRNA,
165 Cas13bt3 initiates an unspecific target-search process involving significant RNA binding that
166 greatly impacts the expression levels of several genes, while a targeting sgRNA narrows the
167 target-search process to reduce overall transcriptomic impact. Notably, despite high levels of
168 overall DEGs, the number of downregulated genes remained similar between the NT sgRNA
169 and VEGFA sgRNA groups suggesting that the NT sgRNA does not induce formation of the
170 catalytic pocket for RNA knockdown, and altered gene expression is predominantly a result of
171 increased RNA binding.

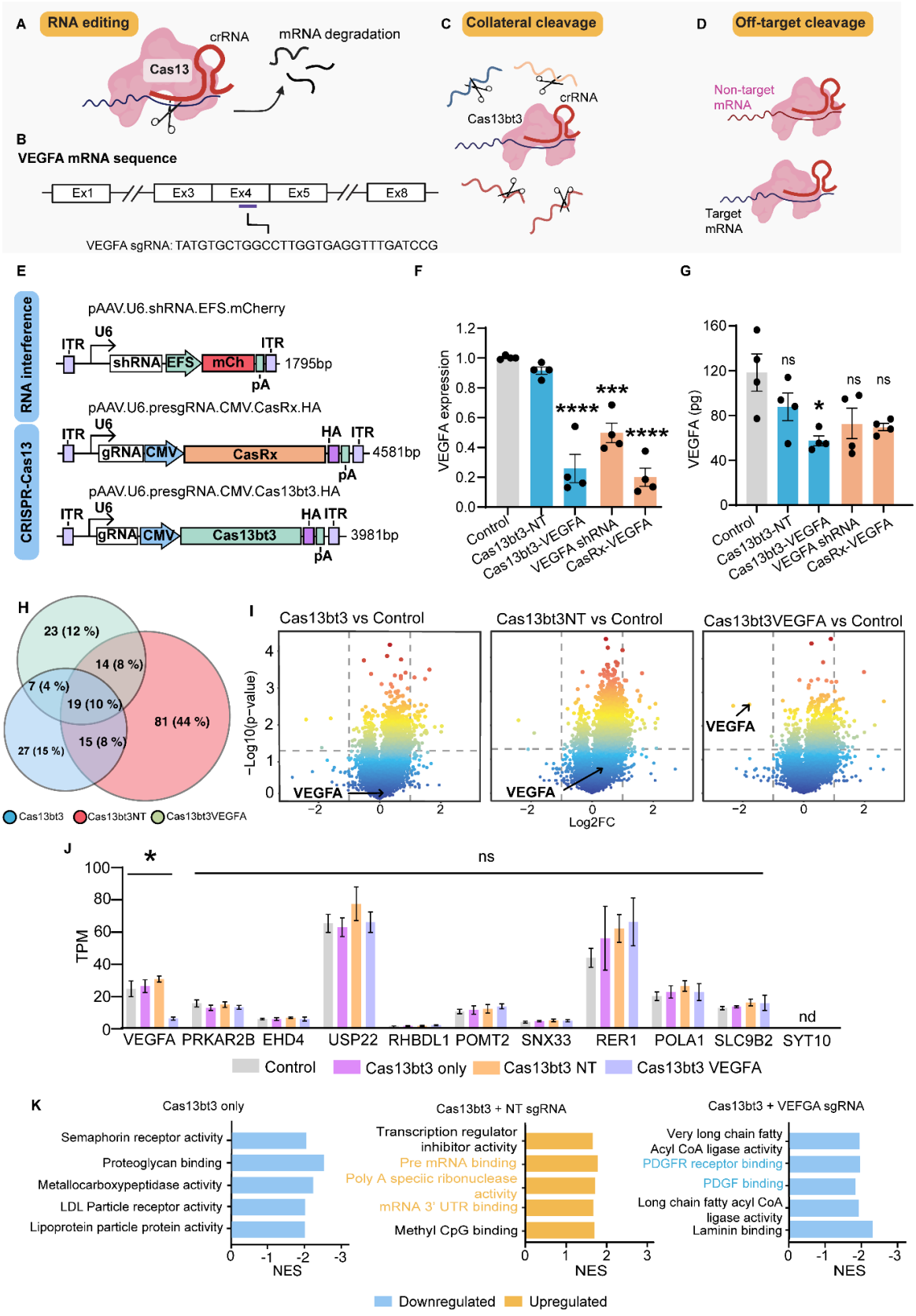
A
RNA editing
crRNA
Cas13
mRNA degradation
B
VEGFA mRNA sequence
Ex1
Ex3
Ex4
Ex5
Ex8
VEGFA sgRNA: TATGTGCTGGCCTTGGTGAGGTTTGATCCG
C
Collateral cleavage
crRNA
Cas13bt3
D
Off-target cleavage
Non-target mRNA
Target mRNA
E
RNA interference
CRISPR-Cas13
pAAV.U6.shRNA.EFS.mCherry
U6
ITR
shRNA
EFS
mCh
ITR
pA
1795bp
pAAV.U6.presgRNA.CMV.CasRx.HA
gRNA
CMV
CasRx
HA
4581bp
pAAV.U6.presgRNA.CMV.Cas13bt3.HA
Cas13bt3
3981bp
F
VEGFA expression
Control
Cas13bt3-NT
Cas13bt3-VEGFA
VEGFA shRNA
CasRx-VEGFA
G
VEGFA (pg)
ns
H
23 (12 %)
14 (8 %)
7 (4 %)
19 (10 %)
81 (44 %)
15 (8 %)
27 (15 %)
Cas13bt3
Cas13bt3NT
Cas13bt3VEGFA
I
Cas13bt3 vs Control
Cas13bt3NT vs Control
Cas13bt3VEGFA vs Control
−Log10(p−value)
Log2FC
VEGFA
J
TPM
VEGFA
PRKAR2B
EHD4
USP22
RHBDL1
POMT2
SNX33
RER1
POLA1
SLC9B2
SYT10
nd
Control
Cas13bt3 only
Cas13bt3 NT
Cas13bt3 VEGFA
K
Cas13bt3 only
Semaphorin receptor activity
Proteoglycan binding
Metallocarboxypeptidase activity
LDL Particle receptor activity
Lipoprotein particle protein activity
Cas13bt3 + NT sgRNA
Transcription regulator inhibitor activity
Pre mRNA binding
Poly A speciic ribonuclease activity
mRNA 3' UTR binding
Methyl CpG binding
Cas13bt3 + VEFGA sgRNA
Very long chain fatty Acyl CoA ligase activity
PDGFR receptor binding
PDGF binding
Long chain fatty acyl CoA ligase activity
Laminin binding
NES
Downregulated
Upregulated

172

173

174 **Fig. 1. Comparison of RNA-targeting tools for in vitro testing of VEGFA mRNA**
175 **silencing. (A)** Schematic of CRISPR-Cas13 mechanism of action. **(B)** VEGFA sgRNA
176 sequence and targeting region on VEGFA mRNA sequence. **(C)** Schematic of collateral and
177 **(D)** off-target cleavage. **(E)** Schematic for domain structure of VEGFA targeting shRNA and
178 Cas13 (CasRx and Cas13bt3) vectors. **(F)** VEGFA mRNA knockdown from shRNA, CasRx
179 and Cas13bt3 in HEK293FT cells (n = 7). **(G)** VEGFA protein expression from ELISA after
180 transfection of shRNA, CasRx and Cas13bt3 plasmids (n = 4). **(H)** Venn diagram of a total
181 number of differentially expressed genes (DEGs) from Cas13bt3 only, Cas13bt3-NT sgRNA
182 and Cas13bt3-VEGFA sgRNA plasmids. **(I)** Volcano plots showing DEGs from Cas13bt3
183 only, Cas13bt3-NT sgRNA and Cas13bt3-VEGFA sgRNA compared to transfection control in
184 HEK293FT cells. VEGFA gene is denoted by a black arrow. **(J)** TPM plot for VEGFA and
185 candidate off-target genes. **(K)** Top 5 enriched GO molecular function (MF) terms from
186 Cas13bt3 only, Cas13bt3-NT sgRNA and Cas13bt3 VEGFA sgRNA. NES above zero
187 represents significant activation of the pathway, while NES below zero represents significant
188 suppression of the pathway. Orange text denotes key factors that are upregulated; blue text
189 denotes key factors that are downregulated. Data presented as mean ± SEM. Statistical analysis
190 was conducted by one-way ANOVA and Tukey's multiple comparison test **(F, G)** and Welch's
191 t-test **(J)**. ns: not significant, *P≤0.05, **P≤0.001, ***P≤0.0001, ****P≤0.00001.

192

193 ***Multiplexing sgRNAs for CRISPR-Cas13bt3 knockdown of target gene from a single-AAV***
194 ***vector***

195 The small size of Cas13bt3 and the significant downregulation of *VEGFA* mRNA observed
196 prompted us to hypothesize that multiple sgRNAs can be delivered using a single AAV vector
197 to increase overall targeting and RNA knockdown efficiency. In theory, multiple sgRNAs
198 would increase rate of Cas13 activation and levels of intracellular Cas13-sgRNA complexes
199 for RNA silencing.

200 To understand Cas13bt3 activation and demonstrate multiplex targeting, we transfected
201 Cas13bt3-VEGFA sgRNA and Cas13bt3 with a VEGFA sgRNA array (carrying three
202 VEGFA-targeting sgRNAs) (**Figure 2A-C**). Surprisingly, cells transfected with Cas13bt3-
203 VEGFA sgRNA or Cas13bt3-VEGFA sgRNA array showed similar levels of significant

204 *VEGFA* mRNA knockdown (<90%) (**Figure 2D,** n = 3 independent experiments). We then
205 sought to study collateral and off-target cleavages from the VEGFA sgRNA array system using
206 RNA-seq. Overall DEGs for both single and multiple sgRNA groups when compared to NT
207 control were comparable and suggested minimal collateral activity from the sgRNA array
208 system (**Figure 2E**). Again, we identified top candidate off-target genes for the other *VEGFA*
209 sgRNAs (**Figure S4B and C**) and did not detect any significant off-target activity in these
210 genes by the Cas13bt3-VEGFA sgRNA array system as well (**Figure 2F**). Active Cas13
211 nucleases competing for target mRNA or low levels of *VEGFA* mRNA transcripts may have
212 resulted in the lack of improvement in targeting efficiency, however our results suggest that
213 multiple sgRNAs can be used simultaneously with Cas13bt3 while still avoiding significant
214 collateral activity.

215 Apart from competition for substrate mRNA, it was recently reported that the presence of "UC"
216 sites on the target mRNA may also affect knockdown efficiency, with "UC" sites within 10-20
217 bases of spacer binding to allow for optimal cleavage (**Figure S3A**)(*16*). We found that while
218 sgRNA1 and sgRNA2 had "UC" sites in these optimal regions, sgRNA3 had only one distal
219 "UC" site 40 nucleotides away from spacer binding (**Figure S3B**). While we did not
220 independently test the knockdown efficiency of our sgRNAs, this finding suggests sgRNA 3
221 alone would achieve low levels of RNA knockdown. As no improved knockdown was
222 observed from the VEGFA sgRNA array, we proceeded to investigate Cas13bt3 with a single
223 sgRNA further.

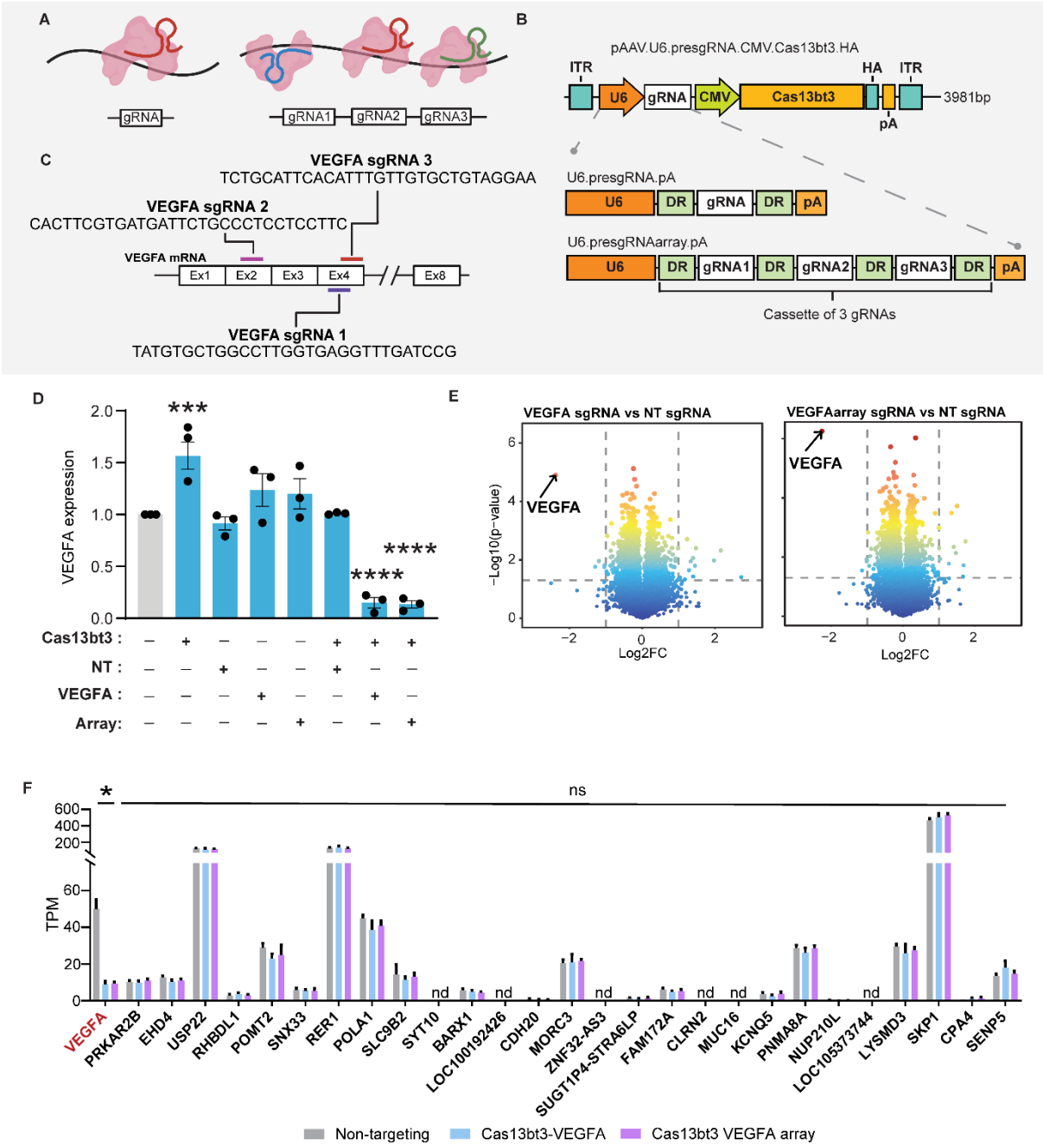
A
gRNA
gRNA1
gRNA2
gRNA3
B
pAAV.U6.presgRNA.CMV.Cas13bt3.HA
ITR
U6
gRNA
CMV
Cas13bt3
HA
ITR
pA
3981bp
U6.presgRNA.pA
U6
DR
gRNA
DR
pA
U6.presgRNAarray.pA
U6
DR
gRNA1
DR
gRNA2
DR
gRNA3
DR
pA
Cassette of 3 gRNAs
C
VEGFA sgRNA 3
TCTGCATTCACATTTGTTGTGCTGTAGGAA
VEGFA sgRNA 2
CACTTCGTGATGATTCTGCCCTCCTCCTTC
VEGFA mRNA
Ex1
Ex2
Ex3
Ex4
Ex8
VEGFA sgRNA 1
TATGTGCTGGCCTTGGTGAGGTTTGATCCG
D
VEGFA expression
2.0
1.5
1.0
0.5
0.0
***
****
****
Cas13bt3 :
NT :
VEGFA :
Array:
E
VEGFA sgRNA vs NT sgRNA
VEGFAarray sgRNA vs NT sgRNA
−Log10(p−value)
Log2FC
VEGFA
F
TPM
ns
VEGFA
PRKAR2B
EHD4
USP22
RHBDL1
POMT2
SNX33
RER1
POLA1
SLC9B2
SYT10
BARX1
LOC100192426
CDH20
MORC3
ZNF32-AS3
SUGT1P4-STRA6LP
FAM172A
CLRN2
MUC16
KCNQ5
PNMA8A
NUP210L
LOC105373744
LYSMD3
SKP1
CPA4
SENP5
nd
Non-targeting
Cas13bt3-VEGFA
Cas13bt3 VEGFA array

224

225

226 **Fig. 2. Guide-dependent and guide-independent off-targets from Cas13bt3-mediated**
227 **VEGFA knockdown. (A)** Schematic of single and multiplex targeting with Cas13bt3 and **(B)**
228 U6-sgRNA domain in single sgRNA and multiple sgRNA vectors. **(C)** Guide RNA targeting
229 regions in VEGFA mRNA. **(D)** VEGFA mRNA knockdown from Cas13bt3, non-targeting and
230 targeting sgRNAs. **(E)** Volcano plots showing differentially expressed genes between
231 Cas13bt3 with non-targeting and **(F)** TPM plots for VEGFA and candidate off-target genes.
232 Target gene VEGFA is highlighted in red. Data presented as mean ± SEM. Statistical analysis
233 was conducted by one-way ANOVA and Tukey's multiple comparison test **(D)** and Welch's t-
234 test **(F)**. ns: not significant, *P≤0.05, ***P≤0.0001, ****P≤0.00001.

235

236 ***AAV2.7m8 delivery efficiently expresses Cas13bt3 in various retinal cells***

237 Human organoids are excellent models for gaining clinically relevant information on new
238 therapeutic agents, as they are derived from human pluripotent stem cells (PSCs) and reproduce
239 morphological, functional and transcriptomic features *in vitro*(*23*). Recently, hESC-derived
240 retinal organoids have been used to investigate eye development and model inherited retinal
241 diseases as well as the testing of novel gene therapies(*24, 25*). While CRISPR-Cas9 has entered
242 the clinic, Cas13-based therapies largely remain at the preclinical stage, and demonstrating
243 utility of Cas13 in retinal organoids will be a major advance for ocular gene therapy.

244 Here we utilised our well-established 2D/3D differentiation protocol to generate hESC-derived
245 retinal organoid containing all the major cell types in the retina(*26*). First, to ensure maximum
246 expression of the Cas13 nuclease in the retinal cells, we subjected the Cas13bt3 protein
247 sequence to codon optimisation to obtain two other variants of Cas13bt3 ($Cas13bt3_{COP1}$ and
248 $Cas13bt3_{COP2}$) (**Figure S5A**). We compared the expression levels of the original Cas13bt3 with
249 $Cas13bt3_{COP1}$ and $Cas13bt3_{COP2}$ by transfection in HEK293FT and ARPE19 cells and found
250 both variants to exhibit increased expression and knockdown efficiency (**Figure S5B, C and**
251 **D**). Among them, $Cas13bt3_{COP1}$ showed the highest expression and was used for subsequent
252 investigation. To elucidate the activity of Cas13bt3 and efficacy for AAV gene therapy RNA
253 editing in *bona fide* human retinal cells we transduced 19 weeks old organoids with
254 AAV2.7m8.U6.NTsgRNA.Cas13bt3 and AAV2.7m8.U6.VEGFAsgRNA.Cas13bt3 viral
255 vectors. Retinal organoids were then harvested for single cell RNA sequencing (scRNA-Seq)

256 6 weeks after treatment (~25 weeks) for (**Figure 3A**). First, we confirmed that the major retinal
257 cell types were clustered similarly across experimental conditions (S1: Untreated; S2:
258 AAV2.7m8.U6.VEGFAsgRNA.Cas13bt3; and S3: AAV2.7m8.U6.NTsgRNA.Cas13bt3)
259 (**Figure 3B**, n = 3 pooled organoids per condition). We used our recently described retinal atlas
260 dataset to determine fidelity of retinal organoids and identified expression of the different
261 retinal cell markers(*27*), confirming exclusive cell-specific expression of the markers (**Figures**
262 **3C and S6, S7**).

263 Next, to examine Cas13bt3 expression in the retinal organoids, we evaluated read numbers and
264 classified cells containing more than 10 reads of Cas13bt3 to be positive for viral infection.
265 Using this threshold, we determined an average transduction efficiency of 18.78% (1403 out
266 of 7467 cells) for the VEGFA sgRNA group and 25.95% (2260 out of 8706 cells) for the NT
267 sgRNA group. Next, we analysed transduction and presence of Cas13bt3 in specific cell types.
268 While all cell types showed noticeable levels of Cas13bt3, RPE cells, in particular, showed
269 high levels of expression with up to 50% of cells containing Cas13bt3 in the VEGFA sgRNA
270 (S2) treatment group. Interestingly, in the NT sgRNA group, only ~15% of RPE cells expressed
271 Cas13bt3, which could owe to varying culture conditions. Bipolar cells showed the least
272 expression of Cas13bt3 (≤10%), while all other cell types showed moderate expression (≤25%)
273 (**Figure 3D**). Overall, our results indicated AAV2.7m8 as a useful delivery vector for cells
274 across retinal cell types.

275 To investigate the impact of the NT sgRNA in retinal cells, we first compared DEGs between
276 cells positive and negative for Cas13bt3 in the retinal organoid that received the
277 AAV2.7m8.U6.NTsgRNA.Cas13bt3. Here, we observed a significant number DEGs across all
278 cell types, and in similar trend to the HEK293FT cells where most DEGs were upregulated
279 genes (**Figure 3E**). Albeit at a lower extent the same pattern was observed in the retinal
280 organoid transduced with AAV2.7m8.U6.VEGFAsgRNA.Cas13bt3 (**Figure 3F**), suggesting
281 that the NT sgRNA exhibited greater impact on the transcriptome. To determine the specific
282 cell types that were more sensitive to Cas13bt3 expression, we identified unique DEGs from
283 each cell type (to remove common effects from AAV delivery and culturing conditions) across
284 the retinal cells and found macroglial and bipolar cells to exhibit the highest DEGs, which was
285 especially higher in the NT sgRNA group (Macroglial - NT: 5571 vs VEGFA: 2928, Bipolar
286 – NT: 3725 vs VEGFA: 1633) (**Figure 3G**).

287 To understand this effect from the NT sgRNA, we further identified DEGs unique to the NT
288 sgRNA and VEGFA sgRNA group and performed GO analysis to identify responses exclusive
289 to the delivered sgRNA. However, ubiquitin protein-like (UBL) associations (e.g., "*UBL ligase*
290 *binding*", "*UBL transferase activity*") were top hits for both groups across macroglial, bipolar,
291 amacrine and RPE cells (**Figure 3H and Data S2**). Ubiquitin processes are often activated in
292 response to immune stress to facilitate the clearing of proteins inside cells (*28*), and our results
293 suggest the delivery of Cas13bt3 with an activating sgRNA (non-targeting or targeting) to
294 significantly elevate the immune response in retinal cells. This stress response is likely higher
295 with the NT sgRNA group due to unspecific RNA binding, causing the increased
296 transcriptomic impact. The strong stress response from all cells to Cas13bt3 delivery is also
297 likely to have made sgRNA-specific responses challenging to distinguish.

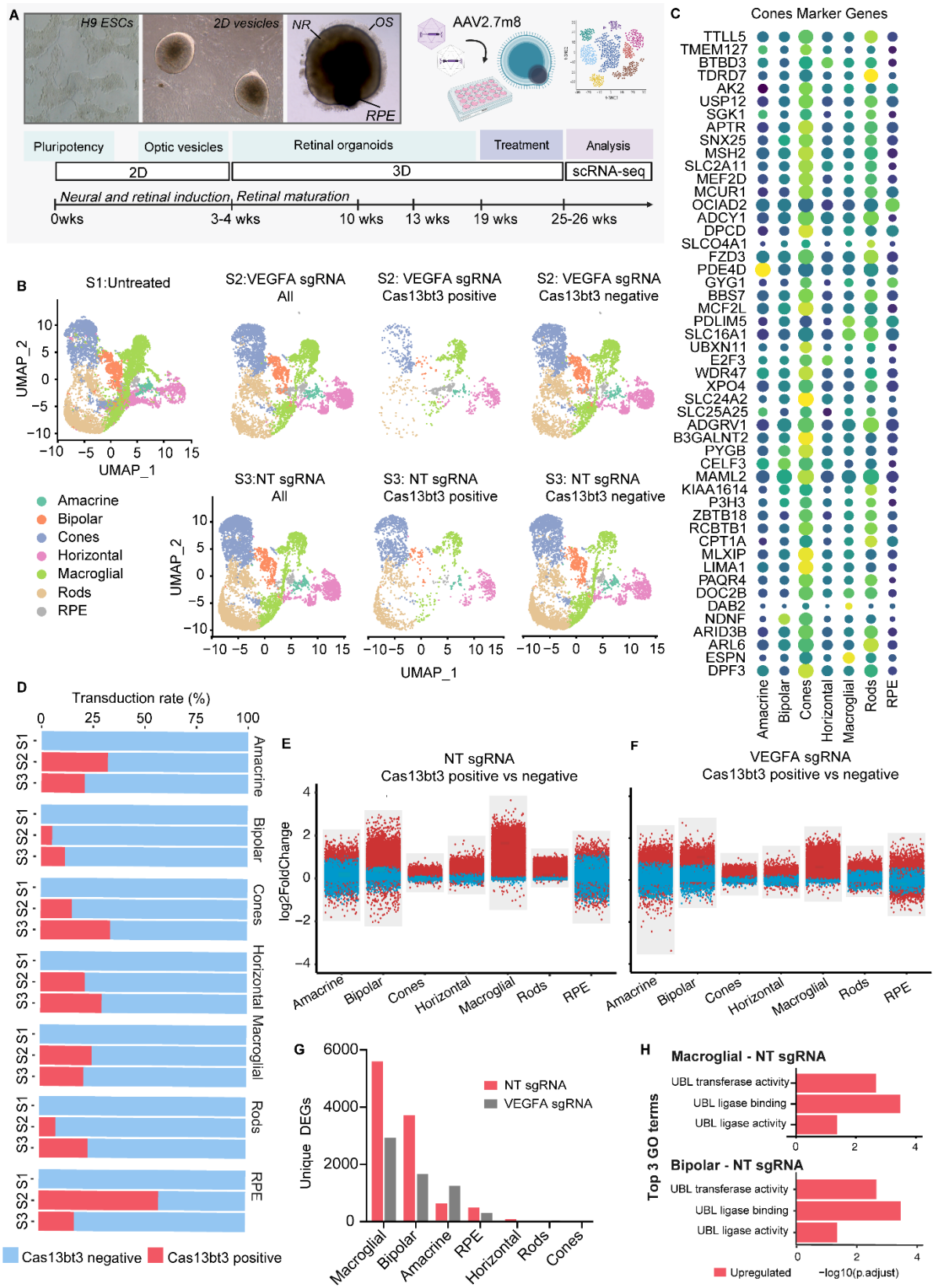
A
H9 ESCs
2D vesicles
NR
OS
RPE
AAV2.7m8
Pluripotency
Optic vesicles
Retinal organoids
Treatment
Analysis
2D
3D
scRNA-seq
Neural and retinal induction
Retinal maturation
0wks
3-4 wks
10 wks
13 wks
19 wks
25-26 wks
B
S1:Untreated
S2:VEGFA sgRNA All
S2: VEGFA sgRNA Cas13bt3 positive
S2: VEGFA sgRNA Cas13bt3 negative
S3:NT sgRNA All
S3: NT sgRNA Cas13bt3 positive
S3: NT sgRNA Cas13bt3 negative
UMAP_1
UMAP_2
Amacrine
Bipolar
Cones
Horizontal
Macroglial
Rods
RPE
C
Cones Marker Genes
TTLL5
TMEM127
BTBD3
TDRD7
AK2
USP12
SGK1
APTR
SNX25
MSH2
SLC2A11
MEF2D
MCUR1
OCIAD2
ADCY1
DPCD
SLCO4A1
FZD3
PDE4D
GYG1
BBS7
MCF2L
PDLIM5
SLC16A1
UBXN11
E2F3
WDR47
XPO4
SLC24A2
SLC25A25
ADGRV1
B3GALNT2
PYGB
CELF3
MAML2
KIAA1614
P3H3
ZBTB18
RCBTB1
CPT1A
MLXIP
LIMA1
PAQR4
DOC2B
DAB2
NDNF
ARID3B
ARL6
ESPN
DPF3
D
Transduction rate (%)
S3 S2 S1
Cas13bt3 negative
Cas13bt3 positive
E
NT sgRNA
Cas13bt3 positive vs negative
log2FoldChange
F
VEGFA sgRNA
Cas13bt3 positive vs negative
G
Unique DEGs
NT sgRNA
VEGFA sgRNA
H
Macroglial - NT sgRNA
UBL transferase activity
UBL ligase binding
UBL ligase activity
Bipolar - NT sgRNA
Top 3 GO terms
Upregulated
-log10(p.adjust)

298

299

300 **Fig. 3. Cas13bt3 treatment and single-cell RNA sequencing of 3D retinal organoids. (A)**
301 Schematic of 3D retinal organoid scRNA-seq experimental procedure. **(B)** UMAP plots show
302 retinal cell type clusters for the untreated, NT sgRNA and VEGFA sgRNA treatment groups.
303 **(C)** Expression of cell-type specific markers in cone cells. **(D)** Infection rate of retinal
304 organoids by cell type and treatment group. **(E)** Multi-volcano plots showing differentially
305 expressed genes (DEGs) between Cas13bt3 positive and negative cells from the NT sgRNA
306 and **(F)** VEGFA sgRNA treatment groups. **(G)** Number of unique DEGs across retinal cell
307 types. **(H)** GO molecular function terms related to unique DEGs from Cas13bt3-NT sgRNA
308 treatment for macroglial and bipolar cells. UBL = Ubiquitin-like protein.

309

310 ***Cas13bt3 can significantly knock down VEGFA mRNA in retinal organoids***

311 Next, we examined Cas13bt3 targeting efficiency and effect on *VEGFA* expression across the
312 retinal cell types. First, we determined *VEGFA* expression in control untreated organoids.
313 *VEGFA* mRNA is present across all retinal organoids cell types. Expression of VEGFA varied
314 significantly between retinal cell types with macroglial, rod, cone photoreceptors, and bipolar
315 cells expressing significantly less *VEGFA* than RPE cells (**Figure S8A, B**).

316 Furthermore, *VEGFA* expression was also detected in all treated organoids, albeit at different
317 levels (**Figure S8C-E**). DEGs were detected in all cell types between retinal organoids
318 transduced with Cas13bt3-VEGFA sgRNA and Cas13bt3-NT sgRNA. However, a significant
319 downregulation of *VEGFA* was only detected in RPE cells (**Figure S9**). While Cas13bt3
320 positive cells have been identified, the abundance of Cas13bt3 reads within cells may still vary
321 (**Figure 4A**) and affect determination of targeting efficiency. We hypothesised that increased
322 intracellular Cas13bt3 transcripts allows for higher targeting efficiency and thereby increased
323 silencing of *VEGFA* mRNA (**Figure 4B**). We first examined the number of Cas13bt3 reads in
324 cells that received AAV2.7m8.U6.NTsgRNA.Cas13bt3 and
325 AAV2.7m8.U6.VEGFAsgRNA.Cas13bt3 treatments (**Figures 4C and S10**). To accurately
326 determine Cas13bt3 effect and to understand abundance of the targeting complex within each
327 cell we examined AAV2.7m8.U6.VEGFAsgRNA.Cas13bt3 treated cells. Here, we found RPE
328 and macroglial cells expressed high levels of Cas13bt3 expression while most cones, rods and
329 horizontal and bipolar cells only showed low levels of Cas13bt3 expression (**Figure 4C**). We

330 selected a threshold to classify high (≥ 50 reads) and low (<50 reads) expression of Cas13bt3
331 that enables evaluation of targeting efficiency. Next, we quantified *VEGFA* mRNA expression
332 in cells expressing high and low levels of Cas13bt3. To this end, we pooled cells within the
333 high and low Cas13bt3 thresholds and compared average *VEGFA* expression against Cas13bt3
334 negative cells to determine if loss of *VEGFA* is from is dependent on high levels of Cas13bt3.
335 Significant decrease of *VEGFA* in high Cas13bt3-expressing cells compared to low Cas13bt3-
336 expressing cells would indicate *VEGFA* silencing from increased targeting activity, while
337 significant reduction compared to negative cells would indicate *VEGFA* loss from viral
338 delivery. Here, we observed that RPE cells were the only cells to show significant reduction of
339 *VEGFA* expression in the high Cas13bt3 when compared to low Cas13bt3 cells ($P < 0.05$)
340 (**Figure 4D**, red square). Viral delivery appeared to upregulate *VEGFA* expression in
341 macroglial cells with both low and high Cas13bt3-expressing cells exhibiting significant
342 increase in VEGFA expression (**Figure 4D**). Interestingly, the increase of *VEGFA* was not
343 significant between low and high Cas13bt3 expressing macroglial cells, suggesting a
344 considerable loss of *VEGFA* (**Figure 4D**). We therefore further investigated retinal cells that
345 showed moderate transduction (~25%) of Cas13bt3-VEGFA sgRNA (i.e. amacrine, horizontal
346 and macroglial) and compared *VEGFA* expression to cells that received Cas13bt3-NTsgRNA.
347 Promisingly, we observed near significant downregulation of *VEGFA* in amacrine and
348 horizontal cells ($P = 0.075$ and $P = 0.051$ respectively), suggesting higher transduction rates
349 may lead to significant downregulation in the other cells as well (**Figure S11**). We then studied
350 DEGs in the RPE cells to determine if the off-target genes previously identified were affected
351 from the significant Cas13bt3-mediated *VEGFA* silencing. Importantly, none of the off-target
352 genes we previously identified were significantly affected (**Figures 4E and S12**). Finally, GO
353 analysis revealed that "*PDGF receptor binding*" was among the top five downregulated
354 processes (**Figure 4F and Data S3**), akin to our observations in HEK293FT cells.

355 While we only observed significant *VEGFA* mRNA knockdown in RPE cells, whether this is
356 a result of higher transduction or RPE cells carry cell-specific factors that are conducive for
357 Cas13 activity needs further investigation. Regardless, with RPE cells being major contributors
358 of *VEGFA* expression, our results show that Cas13bt3 can be a potent tool against diseases
359 such as DR and nAMD.

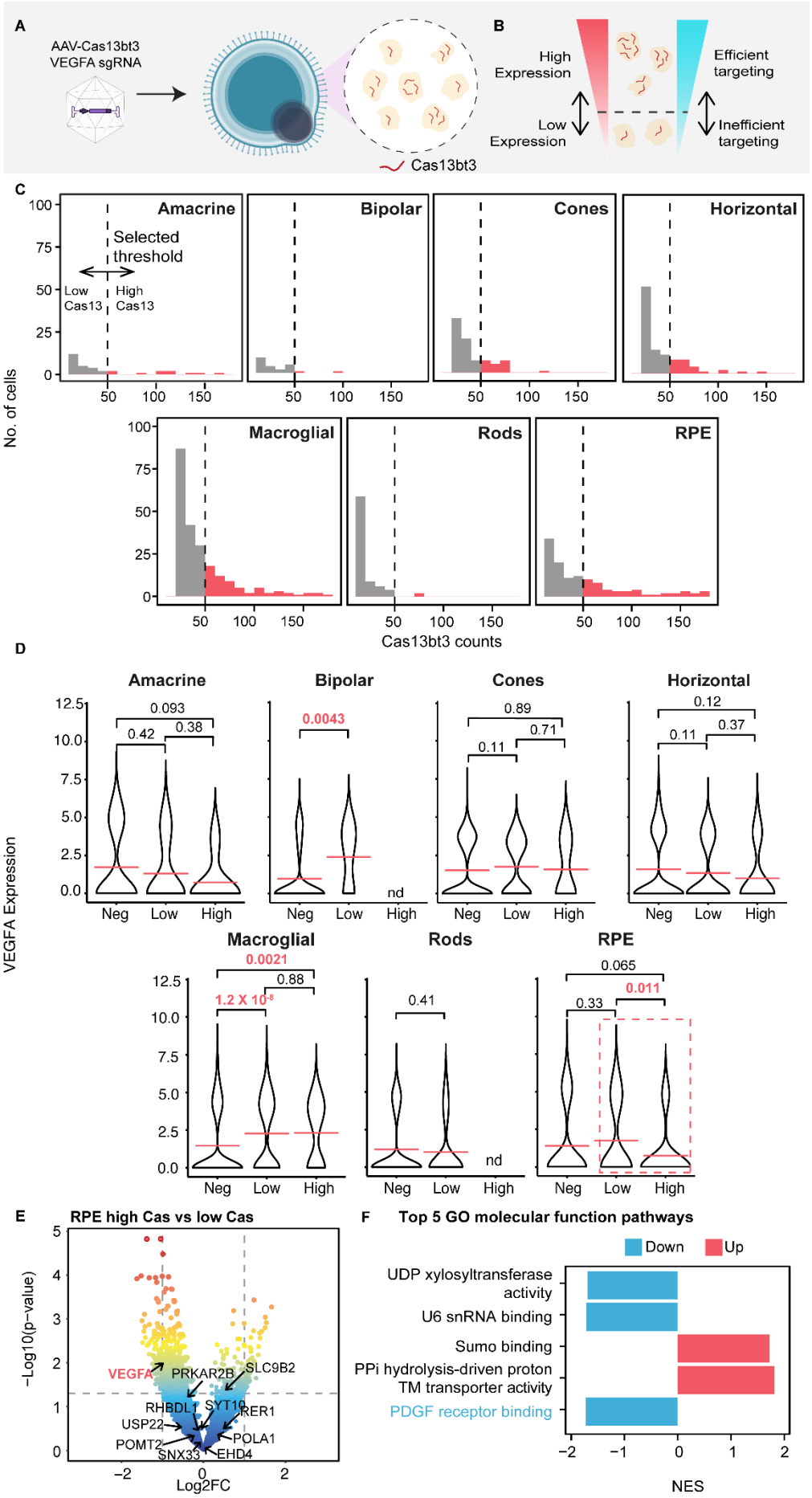
A
AAV-Cas13bt3
VEGFA sgRNA
Cas13bt3
B
High Expression
Low Expression
Efficient targeting
Inefficient targeting
C
Amacrine
Bipolar
Cones
Horizontal
Selected threshold
Low Cas13
High Cas13
No. of cells
Macroglial
Rods
RPE
Cas13bt3 counts
D
VEGFA Expression
Amacrine
Bipolar
Cones
Horizontal
Macroglial
Rods
RPE
Neg
Low
High
nd
E
RPE high Cas vs low Cas
−Log10(p−value)
Log2FC
VEGFA
PRKAR2B
SLC9B2
RHBDL1
SYT10
RER1
USP22
POMT2
SNX33
EHD4
POLA1
F
Top 5 GO molecular function pathways
Down
Up
UDP xylosyltransferase activity
U6 snRNA binding
Sumo binding
PPi hydrolysis-driven proton TM transporter activity
PDGF receptor binding
NES

361 **Fig 4. VEGFA knockdown efficiency in human retinal organoids. (A)** Schematic of
362 variable Cas13bt3 expression in retinal organoid cells and **(B)** relationship between CRISPR-
363 Cas13bt3 expression and targeting efficiency. **(C)** Histograms showing the level of Cas13bt3
364 expression by number of reads across retinal cell types in the VEGFA sgRNA group. **(D)** Violin
365 plots of VEGFA expression against the level of Cas13bt3 expression across retinal cell types
366 compared to Cas13bt3 negative cells. Red box indicates cells of interest for high VEGFA
367 targeting activity. **(E)** Volcano plot of DEGs between RPE cells with high and low Cas13bt3
368 expression. Significant knockdown of VEGFA is highlighted in red. **(F)** Top five significant
369 GO molecular function terms between RPE cells expressing low and high Cas13bt3. Statistical
370 analyses were conducted using Student's t-test **(D)**. PPi: Pyrophosphatase. TM:
371 Transmembrane.

372

373 ***VEGFA* knockdown impedes disease progression in humanised mouse model of**
374 **proliferative diabetic retinopathy**

375 Lastly, we sought to investigate if *VEGFA* knockdown can control neovascularisation *in vivo*
376 in humanised models of DR. This offers a potential new tool against eye diseases causing
377 neovascularisation. To this end, we utilised the trVEGF029 (Kimba) mouse, a humanised
378 transgenic mouse model where the neuroretina overexpresses h*VEGFA* leading to
379 neovascularisation like human proliferative DR(*29*). To ensure that optimal transduction of the
380 retina is being achieved, we delivered a mCherry reporter gene under the control of CMV
381 promoter using the AAV2.7m8 serotype, known to have excellent transduction of the retina,
382 when delivered intravitreally into C57BL/6 mice (**Figure S13A and B**).
383 Immunohistochemistry analysis of AAV2.7m8.CMV.mCherry treated retinal flatmounts
384 showed high levels of fluorescence through all retinal layers (RGCs, bipolar and photoreceptor
385 cells) 4 weeks following injections, confirming quick onset and deep penetration of the retina
386 from intravitreal delivery (**Figure S13C, n = 6 eyes from 3 animals**).

387 Next we treated Kimba mice with AAV2.7m8 viruses driving our codon optimised Cas13bt3
388 carrying NT sgRNA (AAV2.7m8.U6.NTsgRNA.Cas13bt3) or VEGFA sgRNA
389 (AAV2.7m8.U6.VEGFAsgRNA.Cas13bt3). Due to severe disease progression in homozygous
390 Kimba ($VEGFA^{+/+}$), we opted for the heterozygous ($VEGFA^{+/-}$) breed. Six-week-old Kimba

391 mice received bilateral, intravitreal injections of AAV2.7m8.U6.NTsgRNA.Cas13bt3 or
392 AAV2.7m8.U6.VEGFAsgRNA.Cas13bt3. Eight weeks following treatment eyes were
393 analysed for *VEGFA* mRNA expression, neovascular growth, and retinal degeneration (**Figure**
394 **5A**). Similar to the control mCherry treatments, high transduction of photoreceptor cells was
395 observed as demonstrated by co-localisation of mCherry and HA-tag (Cas13bt3) with
396 Rhodopsin positive cells in the ONL (**Figure 5B, C**). In addition qPCR analysis showed high
397 expression of Cas13bt3 in Kimba retinas injected with AAV.2.7m8.U6.NTsgRNA.Cas13bt3
398 and AAV2.7m8.U6.VEGFAsgRNA.Cas13bt3 (**Figure 5D,** n = 3-12 retinas). This
399 corresponded with ~50% reduction ($P < 0.001$) of human VEGFA (*hVEGFA)* mRNA (**Figure**
400 **5E**), but not mouse VEGFA (mVEGFA) (**Figure 5F**) in the
401 AAV2.7m8.U6.VEGFAsgRNA.Cas13bt3 group, while no reduction was observed with
402 AAV2.7m8.U6.NTsgRNA.Cas13bt3 or no treatment (**Figure 5E, F,** n = 3-12 retinas). These
403 results confirmed specific knockdown of *hVEGFA* from Cas13bt3, despite high
404 complementarity of *VEGFA* sequences (29 out of 30 nucleotides) in the targeting region
405 (**Figure 5G**). RNA sequencing further confirmed that mouse VEGFA expression and predicted
406 off-target genes were not significantly altered, indicating safety of Cas13bt3-mediated RNA
407 silencing (**Figure S13**).

408 To confirm if *VEGFA* mRNA knockdown influenced disease progression, we analysed fundus
409 fluorescein angiography (FFA) images from Kimba eyes for vessel leakage and quantified
410 vessel density and number of branch points, which are signs indicative for the neovascular
411 process. We used fluorescein to label vessels of the AAV2.7m8.U6.VEGFAsgRNA.Cas13bt3,
412 AAV2.7m8.U6.NTsgRNA.Cas13bt3 and untreated eyes. We observed large spots of vessel
413 leakage, indicating neovascularisation had progressed in both untreated and NT treated eyes
414 (**Figure 5H,** green expression and white arrows). However, in the
415 AAV2.7m8.U6.VEGFAsgRNA.Cas13bt3 group, no leakage was observed (**Figure 5H,**
416 VEGFA targeting). Immunohistochemistry against laminin was used to image through the
417 retinal vascular layers (superficial, intermediate and deep vascular plexuses) (**Figure S16A**
418 **and B**). Blood vessels appeared diminished in the intermediate and deep vascular layers for
419 the VEGFA sgRNA group. In the NT sgRNA group, the neovascular process could be observed
420 through leaky vessel structure in the same layers (**Figure S16C,** n = 4 retinas). The
421 AAV2.7m8.U6.VEGFAsgRNA.Cas13bt3 treated eyes also showed significantly lower vessel

422 density and branch points compared to baseline at 6 weeks post-treatment, unlike the untreated
423 and the AAV27m8.U6.NTsgRNA.Cas13bt3 eyes (**Figure 5I and J,** n = 4-13 retinas, P<0.05).
424 Next, to determine whether *VEGFA* knockdown leads to rescue of overall retinal structure. we
425 performed optical coherence tomography (OCT) to analyse total retinal thickness (TRT) before
426 and after treatments. We observed no significant changes between the untreated and treated
427 groups, and a general decline in TRT across all animals (**Figure S17**). We postulate that the
428 overexpression of *hVEGFA* promotes rapid retinal degeneration that could not be controlled or
429 reversed through *VEGFA* silencing.

430 Overall, our findings showed Cas13bt3-mediated RNA silencing to significantly reduce
431 *VEGFA* mRNA expression, specifically target *hVEGFA* and control hallmark signs of
432 neovascularisation in a humanised mouse model, promising a useful alternative to current anti-
433 VEGF drugs.

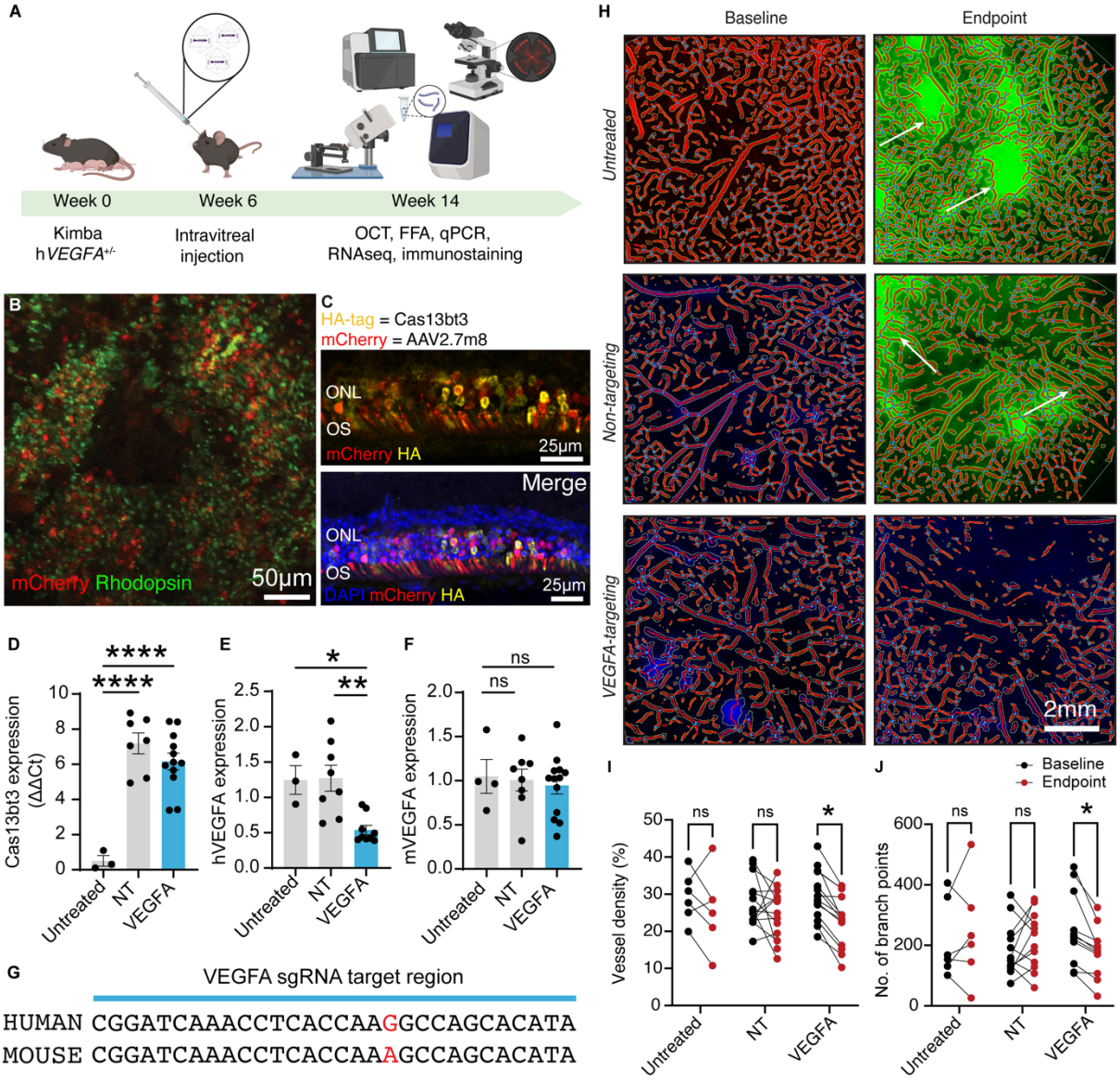
A
Week 0
Week 6
Week 14
Kimba
hVEGFA+/-
Intravitreal
injection
OCT, FFA, qPCR,
RNAseq, immunostaining
B
mCherry Rhodopsin
50µm
C
HA-tag = Cas13bt3
mCherry = AAV2.7m8
ONL
OS
mCherry HA
25µm
Merge
DAPI mCherry HA
D
Cas13bt3 expression (ΔΔCt)
Untreated
NT
VEGFA
E
hVEGFA expression
F
mVEGFA expression
ns
G
VEGFA sgRNA target region
HUMAN CGGATCAAACCTCACCAAGGCCAGCACATA
MOUSE CGGATCAAACCTCACCAAAGCCAGCACATA
H
Baseline
Endpoint
Untreated
Non-targeting
VEGFA-targeting
2mm
I
Vessel density (%)
J
No. of branch points
Baseline
Endpoint

434

435

436 **Fig 5. *In vivo* VEGFA mRNA knockdown in humanised Kimba mice. (A)** Schematic of
437 experimental procedure for intravitreal treatment of Kimba mice. **(B and C)**
438 Immunohistochemistry of retinal flatmount and cryosection showing transduction of
439 AAV2.7m8 and expression of Cas13bt3 (Magnification: 20X and 40X, respectively). **(D)**
440 Expression of Cas13bt3 from Kimba mice retinas. (E) Expression of mouse and human
441 VEGFA mRNA in Kimba retinas. **(F)** VEGFA mRNA targeting regions in human and mouse
442 transcriptome. **(G)** Plot of vessel density and number of branch points from untreated and
443 treated Kimba eyes at baseline (6 weeks) and endpoint (14 weeks) analysed from in vivo central
444 fluorescein fundus angiography (FFA). **(H)** Central fluorescein fundus angiography (FFA)
445 images were obtained from Kimba mice at baseline (6 weeks) and endpoint (14 weeks) after
446 AngioTool analysis and quantification **(I and J)**. Images were edited using Adobe Photoshop
447 to remove central retinal arteries and veins. Green spots and white arrows indicate leakage from
448 blood vessels. Data presented as mean ± SEM. Statistical analysis was conducted by one-way
449 ANOVA with Tukey's multiple comparison test **(D-F)** and Multiple paired t-tests **(I-J)**.
450 *P≤0.05, **P ≤0.001, ****P≤0.00001.

451

452 **Discussion**

453 Our comprehensive *in vitro*, *ex vivo* and *in vivo* characterisation of Cas13bt3 activity and
454 performance in the retina provides novel insights for therapeutic use of the enzyme. Cas13bt3
455 was first described only two years ago but has garnered significant attention for its compact
456 size and reported specificity(*11*). Structural characterisation and activation mechanisms have
457 recently been described spearing immense interest in the molecule for therapeutic
458 development(*16, 30*). Due to ongoing controversy over the exact specificity of Cas13
459 nucleases(*10*), we aimed to characterise Cas13bt3 efficiency and specificity in mouse and
460 human cells. We chose to target the *VEGFA* transcripts, as this growth factor is essential for
461 both physiological and pathological angiogenesis. In the retina, physiological functions include
462 its role as a survival factor for retinal ganglion cells(*31*), photoreceptors, Müller cells(*32*), and
463 RPE(*33*). In disease, overexpression of VEGFA leads to neovascularisation and vision loss.
464 Therefore, clinical applicability of VEGFA downregulation in specific cell types of the retina
465 is of great importance.

466 Previous studies have demonstrated transcript knockdown using CasRx proteins(*11, 12*).
467 Notably, CasRx-mediated *VEGFA* mRNA knockdown has also been shown to reduce choroidal
468 neovascularisation after silencing VEGFA in RPE cells *in vivo* in laser-induced choroidal
469 neovascularisation model(*4*). Our results confirmed that Cas13bt3 mediates significant
470 knockdown of *VEGFA* in human cell lines, hESC-derived retinal cells, and the mouse retina.
471 We further investigated the transcriptomic impact of expressing active Cas13bt3 in the cells
472 and found that initiating Cas13bt3's target search process with a non-targeting sgRNA can lead
473 to significant RNA binding, upregulating the expression of several genes. A targeting sgRNA,
474 such as with VEGFA, appears to narrow the target-search process and thereby reduce
475 transcriptomic impact.

476 *In vitro*, and specifically in HEK293FT cells, several studies have shown Cas13 nucleases to
477 be highly precise(*10*). Most of these studies, however, compared differentially expressed genes
478 to a NT control, not accounting for transcriptomic perturbations from a Cas13-NT sgRNA
479 complex. A recent study showed high collateral activity from CasRx when compared to an
480 empty vector(*34*). Here, we compared targeting Cas13bt3 to vector controls showing minimal,
481 but positive collateral activity. More importantly, we show that Cas13 with a NT sgRNA has
482 significant transcriptomic impact resulting in high levels of DEGs. This demonstrates that NT
483 sgRNAs are not appropriate controls for determining specificity of Cas13 nucleases raising
484 awareness against their use.

485 We also show that multiple sgRNAs can be incorporated within a single AAV vector with
486 Cas13bt3 driven by a strong ubiquitous promoter (CMV) for targeted knockdown of *VEGFA*
487 mRNA. Even though this appears to be an attractive approach to enhance transcript knockdown
488 our study established that multiple sgRNAs failed to improve transcript degradation. The rate
489 of mRNA knockdown was comparable to single sgRNA treatments. Previously, we similarly
490 observed with multiplexed RNA editing with CasRx carrying three *VEGFA*-targeting sgRNAs,
491 the multiple sgRNA system unexpectedly led to decreased knockdown efficiency(*19*), raising
492 the suspicion that substrate competition or inadequate Cas13 activation plays an inhibitory role
493 in RNA targeting efficiency. Interestingly, the comparable levels of DEGs in both single and
494 multiple sgRNA vectors suggest that Cas13bt3 activation is not drastically elevated with the
495 presence of additional sgRNAs. While we did not investigate the delivery of sgRNAs targeting
496 multiple genes, our results show multiple sgRNAs do not increase overall collateral activity,

497 which might prove useful when several genes must be targeted simultaneously to control
498 disease progression. This approach could potentially be applied even to ocular
499 neovascularisation by simultaneously targeting the *VEGFA* and *PDGF* genes for enhanced
500 treatment(*35*).

501 Furthermore, we investigated for the first time AAV-mediated Cas13 RNA expression and
502 editing in retinal organoids at single cell resolution. While several studies have demonstrated
503 *VEGFA* silencing for control of neovascularisation, previous studies have focused on specific
504 cell types that are believed to be major contributors to *VEGFA* expression, like RPE and Müller
505 cells(*4, 36*). While this proves useful to demonstrate proof-of-concept, it does not provide a
506 comprehensive understanding relevant for therapeutic development as *VEGFA* silencing in one
507 cell type may have collateral effects on other retinal cells. Retinal organoid models enable the
508 testing of therapies in an environment that mimics the human retina containing lamination and
509 major retinal cell types of the developing retina. Here we sought to understand retina-wide
510 effect following delivery of Cas13bt3 as well as targeted silencing of *VEGFA*. Our findings not
511 only support the use of Cas13bt3 for ocular gene therapy, but also brings to light several
512 considerations for its use. First, we showed transduction across all retinal cell types studied
513 with the clinically relevant AAV2.7m8 vector (NCT04418427) confirming its effectiveness as
514 a vector for retinal transduction and supporting its clinical utility(*37, 38*). Among the retinal
515 cell types studied, bipolar cells showed the least transduction by AAV2.7m8, while RPE cells
516 seemed more susceptible. It is likely that these differences are due to cell-specific transduction
517 susceptibility, as RPE cells are easily transduced with a variety of AAV capsids(*39*). It should
518 also be noted that overall transduction was determined using an arbitrary cut-off (Cas13bt3
519 read counts ≥ 10) based on our previous experience with the retinal organoids(*26*). NT sgRNA
520 activity following gene therapy led to numerous DEGs when compared to VEGFA targeted
521 sgRNA. This emphasises the need for a well-designed targeting sgRNA for reduced collateral
522 activity. Retinal organoids showed significantly more DEGs than HEK293FT cells, which is
523 expected partly due to cellular response to virus delivery. Still, notwithstanding response to
524 AAV, the higher DEG levels also indicate that retinal cells are more sensitive to Cas13,
525 demonstrating the importance of studying nuclease activity and efficiency in physiological
526 relevant models, an important consideration for Cas-mediated gene therapies. As preclinical
527 studies with Cas13 nucleases are commonly performed in HEK293FT cells, its specificity has

528 often been exaggerated in the literature. Our results strongly suggest that Cas13 specificity
529 must be evaluated in relation to untreated or empty vector controls in organ-specific cells to
530 accurately determine safety. On the front of therapeutic potential, we could only confirm
531 significant targeted *VEGFA* mRNA knockdown in RPE cells, which is likely due to strong
532 expression of Cas13bt3 in these cells. Lower copies of Cas13bt3 in the other cells may have
533 resulted in the lack of significant *VEGFA* knockdown, and further studies are required to
534 understand the levels of Cas13 expression necessary in other retinal cells for effective activity.
535 Testing of cell type specific promoters could be beneficial as CMV promoter is known for its
536 susceptibility to silencing in certain cell types, for example stage specific PSC-derived
537 photoreceptor cells (REF). Importantly, with RPE cells being the primary producers of *VEGFA*
538 in the retina, the significant downregulation of *VEGFA* mRNA in RPE strongly suggests the
539 benefits of Cas13bt3 gene therapy as a potential anti-VEGF tool for neovascular eye disease.

540 Lastly, we tested the anti-VEGF potential of Cas13bt3 in the retina of a humanised mouse
541 model of diabetic retinopathy, the Kimba mouse. We opted to examine anti-VEGF potential of
542 Cas13bt3 in Kimba mice as it shows chronic disease and all major signs of proliferative
543 retinopathy (*29*). Importantly, as Kimba mice expresses human *VEGFA*, the same vectors
544 tested in retinal organoids could also be used *in vivo*. Others have shown the control of ocular
545 neovascularisation using mouse models of laser-induced injury(*4*), streptozotocin (STZ)-
546 induced diabetes(*40*), or oxygen-induced retinopathy (OIR)(*41*). However, these models have
547 some drawbacks. The laser-induced choroidal neovascularisation model often used in anti-
548 VEGF preclinical studies does not accurate model the chronic retinal degeneration observed in
549 DR and nAMD patients and presents *VEGFA* overexpression only as a response to injury(*42*).
550 Diabetic mouse models do not recapitulate proliferative retinopathy which is often the cause
551 of severe vision impairment. Vascular pathogenesis is also delayed and varied based on
552 response to STZ(*43*). OIR mouse models rapidly present proliferative retinopathy, however
553 neovascularisation regresses within a week(*44*).

554 Following RNA editing gene therapy in Kimba retinas, we demonstrated the specific
555 knockdown of human *VEGFA*, with no significant impact on endogenous mouse *VEGFA*. This
556 shows strong evidence for the specificity of targeted Cas13bt3 activity. Silencing of Cas13bt3
557 VEGFA also rescued vascular phenotypes showing an improvement in controlling vascular
558 growth and leakiness. The major concern with current anti-VEGF treatment is the need for

559 frequent intravitreal injections. Recent efforts to address this problem have employed gene
560 editing strategies like targeting *VEGFA* using CRISPR-Cas9 (*36, 45*). However, efficacy of
561 such treatments are limited by efficient and safe delivery of vectors due to the size of Cas9(*46,*
562 *47*), poor efficiency of compact Cas9 nucleases(*48*) or have reported the risk of genomic
563 alterations from long-term expression of Cas9(*49*). Our results indicate that a single intravitreal
564 injection could achieve durable and potent while reversible silencing of *VEGFA*, addressing
565 drawbacks with current gene editing strategies. While RNA editing is thought to be safer than
566 DNA-targeting options, it is prudent to consider effects of long-term Cas13 expression, and
567 Cas13 systems amenable to regulation are of consideration for therapeutic development.

568 There are a few limitations to our study. First, we did not extensively study Cas13bt3
569 expression in ARPE19 cells, where we also observed potent knockdown. While HEK293FT
570 appears resistant to high levels of collateral activity, ARPE19 cells may exhibit significantly
571 higher levels of transcriptomic effects. This is supported by the high levels of DEGs we
572 observed in various cells from the retinal organoids, suggesting significant inflammatory
573 responses as well as cell-specific collateral activity. Specifically, the upregulation of UBL
574 processes across cell types regardless of VEGFA silencing, strongly indicate increased cellular
575 stress from delivery of Cas13. As RNA targeting molecules like Cas13 require persistent
576 expression for therapeutic effect, this could pose a significant safety concern. Second, while
577 vessel density and branching were noticeably reduced, we could not extensively study recovery
578 of phenotype in our mouse model due to severity of the disease. OCT readings showed
579 significant retinal degeneration at treatment timepoint, making rescue of phenotype
580 challenging to assess. Lastly, we were also unable to confirm reduction of VEGFA protein
581 from the mice retinas as not enough protein could be obtained for quantitative analysis.

582 CRISPR-Cas technology has advanced at breakneck speed in the last decade revolutionising
583 medicine and offering potential treatment opportunities to numerous previously incurable
584 diseases. The recent FDA approval of an *ex vivo* CRISPR therapy for sickle-cell disease
585 (branded Casgevy) is evidence of this progress. However, a comprehensive understanding of
586 the CRISPR nucleases is crucial. In this study we offer novel insights into Cas13 targeting
587 mechanisms and its utility in targeting retinal and RPE cells providing evidence for the
588 potential of Cas13-based therapies for ocular disease. This study demonstrated that the
589 hypercompact Cas13bt3 can be efficiently delivered and expressed in various retinal cell types

590 effectively controlling *VEGFA* expression and neovascularisation. In-depth evaluation of
591 collateral activity in retinal cells would facilitate development of a safe and effective Cas13-
592 mediated anti-VEGF AAV gene therapy.

593

594 **Materials and Methods**

595

596 ***Plasmid construction***

597 The protein sequences of CasRx and Cas13bt3 were gifts from P. Hsu(*50*) and H. Yang(*11*),
598 respectively. Cas13bt3 was codon optimised using online tools from Integrated DNA
599 Technologies (IDT), GenScript and Benchling. The all-in-one AAV plasmids for shRNA,
600 CasRx and Cas13bt3 were designed as previously described(*19*), and synthesised by
601 GenScript. All plasmids used in this study are available from Addgene.

602

603 ***Cell culture and transfections***

604 HEK293FT cells (American Type Culture Collection, ATCC) were maintained in Dulbecco's
605 Modified Eagle's Medium (DMEM; Thermo Fisher Scientific) supplemented with 10% (v/v)
606 fetal bovine serum (FBS, Bovogen Biologicals) and 1% (v/v) antibiotic-antimycotic (Thermo
607 Fisher Scientific) in a humidified 5% CO_2 incubator at 37°C. ARPE19 (ATCC) cells were
608 maintained in DMEM/F-12 (Thermo Fisher Scientific) supplemented with 10% (v/v) FBS and
609 1% (v/v) antibiotic-antimycotic.

610

611 ***RT-qPCR***

612 At 48 hours after transfection, RNA was extracted from cells using the Monarch® Total RNA
613 Miniprep Kit (New England Biolabs and 200ng of RNA was converted to complementary DNA
614 (cDNA) using High-Capacity cDNA Reverse Transcription Kit (Thermo Fisher Scientific)
615 according to the manufacturers' instructions. cDNA was diluted with water at the ratio of 1:10.
616 qPCR was performed with 2uL of cDNA using the TaqMan™ Fast Advanced Master Mix
617 (Thermo Fisher Scientific) according to manufacturers' instructions with the following

618 TaqMan probes human VEGFA (Hs00900055_m1; Thermo Fisher Scientific), mouse VEGFA
619 (Mm00437306_m1; Thermo Fisher Scientific), human GAPDH (Hs02786624_g1; Thermo
620 Fisher Scientific), mouse GAPDH (Mm99999915_g1, Thermo Fisher Scientific). Mouse
621 eyeballs were enucleated and stored in 4°C in RNALater® until dissection. Retina was dissected
622 from injected animals and placed in lysis buffer and sonicated for 2 seconds prior to RNA
623 extraction and qPCR as previously described.

624

625 ***Western blot***

626 At 48 hours after transfection, cells were harvested and collected in Pierce™ RIPA buffer
627 (Thermo Fisher Scientific) containing Pierce™ Phosphatase Inhibitor Mini Tablets (Thermo
628 Fisher Scientific). Cell lysate was sonicated for 5 seconds and centrifuged for 15 minutes at
629 13300rpm at 4°C. The supernatant was collected, and protein levels were quantified using the
630 Pierce™ BCA Protein Assay Kit (Thermo Fisher Scientific) as per manufacturers' instructions.
631 For Western blot, 10µg of protein mixed with NuPAGE™ LDS Sample Buffer (4X) (Thermo
632 Fisher Scientific) and loaded in NuPAGE™ 4 to 12% Mini Protein Gel (Thermo Fisher
633 Scientific) for gel electrophoresis at 150V for 30 minutes. Transfer to Amersham™ Hybond™
634 PVDF membrane (Cytiva) was performed at 30V for 1 hour. Protein blot was blocked with 5%
635 skim milk for 1 hour, followed by incubation with HA-tag (C29F4) Rabbit mAb (Cell Signaling
636 Technology®) or Anti-Actin Antibody, clone C4 (Merck) overnight at 4°C. Blots were then
637 stained with Goat anti-Mouse IgG (H+L) Cross-Adsorbed Secondary Antibody, HRP
638 (Invitrogen™) or Goat anti-Rabbit IgG (H+L) Secondary Antibody, HRP (Invitrogen™) for 2
639 hours at room temperature. Blot was incubated with Pierce™ ECL Western Blotting Substrate
640 for 1 minute before imaging using Bio-Rad ChemiDoc. All washes were performed with 1X
641 PBST for 5 minutes, repeated 3 times.

642

643 ***ELISA***

644 At 48 hours after transfection, 100µL of supernatant was collected and ELISA was performed
645 using the Human VEGF DuoSet ELISA (R & D Systems) as per manufacturers' instructions.
646 Briefly, 96-well plates were incubated with Capture Antibody in ELISA Plate coating buffer
647 overnight at room temperature. Plates were then blocked with Reagent Diluent for 1 hour at

648 room temperature, and 100uL of supernatant was incubated for 2 hours at room temperature.
649 Then, Detection antibody was added and incubated for 2 hours at room temperature. After
650 incubation with Streptavidin-HRP and Substrate reagent for 20 minutes each, the provided stop
651 solution was added, and plate was read using the Tecan Spark® Micro plate reader at 450nm
652 with reference wavelength 570nm.

653

654 ***Immunohistochemistry***

655 Retinal flatmounts were washed with 1X PBS containing 0.5% Triton-X-100 (PBST) and
656 permeabilised in -80°C for 15 minutes. After washing with PBST, flatmounts were incubated
657 in anti-rhodopsin antibody (1:500; Abcam) with 2% donkey serum and 2% PBST in 4°C for
658 72 hours. This was followed by incubation in Alexa Fluor 488 AffiniPure Donkey Anti-Mouse
659 IgG (H+L) (1:500; Jackson ImmunoResearch) at room temperature for 2 hours. After washing,
660 the flatmounts were stained with Anti-Laminin-2 (α-2 Chain) antibody, Rat monoclonal (1:250;
661 Merck) and incubated in 4°C for 5 nights. This was followed by incubation in Alexa Fluor®
662 647 AffiniPure Donkey Anti-Rat IgG (H+L) (1:250; Jackson ImmunoResearch) at room
663 temperature for 2 hours. Then, the retinae were washed and incubated in mCherry Monoclonal
664 Antibody (16D7), Alexa Fluor 594 (1:500; Thermo Fisher Scientific) at 4°C for 72 hours.
665 Retinal cryosections were blocked using serum-free protein block (Agilent Dako) at room
666 temperature for 1 hour, followed by incubation at 4°C overnight with primary antibody as
667 previously described. Secondary antibody incubation was performed at room temperature for
668 1 hour as previously described. Slides were stained with NucBlue™ Live ReadyProbes™
669 Reagent (Hoechst 33342; Thermo Fisher Scientific) for 10 minutes before mounting as
670 previously described and imaged on the Stellaris 5 confocal microscope.

671

672 ***hESC Maintenance and Retinal Differentiation Culture***

673

674 hESCs were maintained on feeder-free conditions on E8 (Thermo Fisher) and Geltrex-coated
675 six-well plates. In brief, for retinal differentiation hESCs were maintained until 90%–95%
676 confluent, then FGF-free medium was added to the cultures for 2 days followed by a neural

677 induction period where RPE and retinal vesicles appeared. NRVs were excised and kept in low
678 binding 96-well plates for maturation.

679

680 ***AAV transduction of retinal organoids***

681

682 Retinal organoids were maintained in ALT90 medium as previously described (West et al.,
683 2022) and AAV transduction was performed during the 15-19 weeks of differentiation. On the
684 day of transduction, AAV vectors were diluted in 300µL of fresh ALT90 medium at titer of
685 1x10E11 vg/organoids. The following day treated wells were supplemented with 700µL of
686 fresh ALT90 medium. Transduced organoids were incubated for 72 hours in the AAV vector-
687 containing medium. After the 72-hour incubation, the vector-containing medium was aspirated,
688 and 1mL of fresh ALT90 medium was added to each well. Transduced organoids underwent 6
689 weeks culture until harvesting for experimental procedures.

690

691 ***Immunohistochemistry of retinal organoids***

692 Retinal organoids were fixed for 45 minutes in 4% paraformaldehyde and incubated overnight
693 in 20% sucrose, prior to embedding in OCT. Cryosections (14 µm thick) were collected for
694 analysis and preserved at - 20°C. Cryosections were blocked in 5% goat serum and 1% bovine
695 serum albumin in PBS for 2 hours. Primary antibodies (ARR3: 1:200, Rhodopsin: 1:1000,
696 VSX2: 1:200, CRALBP: 1:200, PROX1:1:200, and HuCHuD:1:500) were incubated overnight
697 at 4°C in blocking solution with 5% goat or donkey serum. After washing of primary antibody
698 with PBS sections were incubated with secondary antibody in blocking solution for 2 hours at
699 RT, washed and counter-stained with DAPI (Sigma-Aldrich). Alexa fluor 488 and 546
700 secondary antibodies (Thermo Fisher Scientific) were used at a 1:500 dilution.

701

702 ***Intravitreal injections***

703 All animal procedures were approved by the Animal Ethics Committees of University of
704 Melbourne and conducted in accordance with The Association for Research in Vision and

705 Ophthalmology (ARVO) Statement for the Use of Animal in Ophthalmic and Vision Research.
706 Ethics approval was obtained from The Florey Institute of Neuroscience and Mental Health
707 Animal Ethics Committee (22-036-UM). The Akimba mice developed by Rakoczy *et al*. (*51*)
708 and the heterozygous Kimba mice (*hVEGFA*$^{+/-}$) were used for this study. Mice were bred in the
709 Melbourne Brain Centre animal facility (Kenneth Myer Building, Parkville, VIC, Australia),
710 and were housed in a well-ventilated environment that was kept at a constant room temperature
711 of 21°C, with a 12-hour diurnal light-dark cycle (lights on: 7am, off: 7pm; room illumination
712 < 50 lux). Mouse chow (Barastoc, Melbourne, VIC, Australia) and water were provided ad
713 libitum. 6-week-old Kimba mice were anesthetized with ketamine (80mg/kg) and xylazine
714 (10mg/kg) solution mix (Troy Laboratory, Smithfield, NSW, Australia; i.p. with 30G needle)
715 and given a drop of 0.5% proxymethacaine hydrochloride (Alcaine™, Alcon Laboratories,
716 Frenchs Forest, NSW, Australia) and 0.5% tropicamide (Mydriacyl™, Alcon Laboratories).
717 Baseline fundus fluoresceine angiography (FFA) were taken (as described below), and animals
718 intravitreally injected with 1uL of AAV2.7m8 viruses using Hamilton syringe attached to a 33-
719 gauge dental needle. Post injection, mice were subcutaneously administered 0.3mL of
720 atipamezole hydrochloride (0.25mg/mL) and allowed to recover on heating pads with food and
721 water *ad libitum*.

722

723 ***Fundus fluorescein angiography and optical coherence tomography***

724 Retinal vasculature was assayed at baseline prior to intravitreal injection of AAVs and 8 weeks
725 after AAV-treatment using fundus fluorescein angiography (FFA) (Spectralis, Heidelberg
726 Engineering, Heidelberg, Germany) immediately after intraperitoneal injection of sodium
727 fluorescein (1%, 100 µL/kg, fluorescite 10%; Alcon Laboratories). Five images (central, nasal
728 superior, temporal superior, nasal inferior, and temporal inferior) were obtained for each eye
729 and analysed using AngioTool(*52*) for vessel density and branch points using default settings.

730 *In vivo* retinal structure was assayed with spectral domain optical coherence tomography (SD-
731 OCT) (Spectralis®, Heidelberg Engineering, Heidelberg, Germany) with general anaesthesia,
732 mydriasis and corneal hydration (Systane, Alcon Laboratories) maintained. During image
733 acquisition, retinal volumes (8.1 × 8.1 × 1.9 mm) centred on the optic nerve head were acquired
734 each consisting of 121 evenly spaced horizontal B-scans. Each B-scan comprised of 768 A-

735 scans with 3.87 µm axial depth resolution, 9.8 µm lateral resolution. OCT scans were captured
736 with an automated real-time tracking average of 6 frames, at an average speed of 85,000 A-
737 scans per second. The Heidelberg Eye Explorer 2 OCT reader plugin (Heidelberg Engineering)
738 was used for analysis. All retinal layers (retinal nerve fibre layer, RNFL; ganglion cell inner
739 plexiform layer, GCIPL; inner nuclear layer, INL; outer plexiform layer, OPL; outer nuclear
740 layer, ONL; photoreceptor segments, PR segment) as well as total retinal thickness (TRT) were
741 automatically segmented (Heidelberg Eye Explorer 2 software). A circular ring around the
742 optic nerve head (Early Treatment Diabetic Retinopathy Study [ETDRS] outer ring) was
743 employed for analysis.

744

745 ***Determination of candidate off-target genes***

746 Off-targets of the gRNAs were predicted using a sequence-based approach. gRNAs in length
747 of 30 bps were first aligned to the human transcriptome (Grch38 cdna from emsembl release
748 100) using blastn (megablast). Flexible options were set to capture the potential offtargets
749 which could tolerate up to 7 mismatches in this step, i.e., max_target_seqs = 10000, evalue =
750 10000, word_size = 5, perc_identity = 0.6. Secondly, the candidates were further filtered with
751 the threshold that at least 13 bp perfect match should exist in each alignment.

752

753 ***Bulk RNA-seq data analysis***

754 Raw data processing was performed using FASTQC (*53*) to check the reads quality and
755 Trimmomatic (*54*) tool to further remove the bases and reads with low quality, adaptors and
756 barcodes. The clean reads were aligned to the reference human genome (version GRCh38),
757 utilizing STAR v2.7 (*55*) as the aligner. For RNA quantification, RSEM (*56*) was employed to
758 normalize raw read counts, transforming them into TPM (transcripts per million) values,
759 providing a relative expression level that is theoretically comparable across samples. The
760 magnitude (log2-transformed fold change) and significance (P-value) of differential expression
761 between groups were then calculated. Differentially expressed genes (DEGs) were selected
762 based on the criteria of a p-value < 0.05 and $|\log2 \text{ fold change}| \geq 1$. Gene set enrichment analysis
763 (GSEA) (*57*), focused on Gene Ontology(*58*), was conducted using the R 4.3.1 Bioconductor
764 package clusterProfiler(*59*) to elucidate whole transcriptomic patterns between groups. To

765 account for multiple testing, P-values underwent adjustment through the Benjamini-Hochberg
766 false discovery rate (BH-FDR).

767

768 ***Single-cell RNA-seq data analysis***

769 After checking the reads quality, the sequencing files were aligned to reference human genome
770 (version GRCh38) using 10X Genomics CellRanger software (v7.1.0) count pipeline to remove
771 non-cellular barcodes and keep the cellular barcodes and gene matrix. To further distinguish
772 the Cas13bt3-valid and -invalid cells, FASTX-toolkit (*60*) was used to keep the reads with
773 cellular barcodes and convert FASTAQ file into FASTA file. Then, Blastn (*61*) was used to
774 compute the similarity between cellular reads and Cas13bt3 reference sequence.
775 Based on the quality of the sequencing reads, appropriate cutoff values for both the percentage
776 of identical positions and the alignment length were employed to delineate cells as either
777 Cas13bt3-valid or Cas13bt3-invalid. For either Cas13bt3-valid or -invalid cells, we further
778 used Seurat v4.3 for data pre-processing, data normalization, feature selection, data scaling,
779 dimensional reduction and clustering. To refine the characterization of cell types within each
780 cluster, ScType (*62*) was employed, leveraging genesets specific to eight retinal cell types—
781 amacrine, bipolar, cones, horizontal, macroglial, microglial, rods, and RPE—validated by Kim
782 et al. (*27*). The magnitude (log2-transformed fold change) and significance (P-value) of
783 differential expression between cell types were then calculated. Differentially expressed genes
784 (DEGs) were selected based on the criteria of a p-value < 0.05 and $|\log2 \text{ fold change}| \geq 1$. Gene
785 set enrichment analysis (GSEA) (*57*), focused on Gene Ontology (*58*), was conducted using
786 the R 4.3.1 Bioconductor package clusterProfiler (*59*) to elucidate whole transcriptomic
787 patterns between groups. To account for multiple testing, P-values underwent adjustment
788 through the Benjamini-Hochberg false discovery rate (BH-FDR).

789

790 ***Statistical analysis***

791 Statistical analyses were performed using GraphPad Prism 10. Analytical methods are
792 described in respective figure legends with *p*-value indicators. For *ex vivo* studies, to assess the
793 strength of the relationship between gene expression values and the number of Cas13bt3-valid
794 read counts following log2 transformation in each cell type, Spearman's rank correlation

795 coefficient was employed. The associated *p-value* serves as an indicator of the likelihood or
796 probability that any observed correlation is merely a result of chance.

797

798

799 **References**

800

801 1. J. Y. Wang, J. A. Doudna, CRISPR technology: A decade of genome editing is only
802 the beginning. *Science* **379**, eadd8643 (2023).
803 2. S. Kumar, L. E. Fry, J.-H. Wang, K. R. Martin, A. W. Hewitt, F. K. Chen, G.-S. Liu,
804 RNA-targeting strategies as a platform for ocular gene therapy. *Prog. Retin. Eye Res.*
805 **92**, 101110 (2023).
806 3. Y. Hu, Y. Chen, J. Xu, X. Wang, S. Luo, B. Mao, Q. Zhou, W. Li, Metagenomic
807 discovery of novel CRISPR-Cas13 systems. *Cell Discovery* **8**, 107 (2022).
808 4. C. Zhou, X. Hu, C. Tang, W. Liu, S. Wang, Y. Zhou, Q. Zhao, Q. Bo, L. Shi, X. Sun,
809 H. Zhou, H. Yang, CasRx-mediated RNA targeting prevents choroidal
810 neovascularization in a mouse model of age-related macular degeneration. *Natl. Sci.*
811 *Rev.* **7**, 835-837 (2020).
812 5. H. Zhou, J. Su, X. Hu, C. Zhou, H. Li, Z. Chen, Q. Xiao, B. Wang, W. Wu, Y. Sun,
813 Y. Zhou, C. Tang, F. Liu, L. Wang, C. Feng, M. Liu, S. Li, Y. Zhang, H. Xu, H. Yao,
814 L. Shi, H. Yang, Glia-to-Neuron Conversion by CRISPR-CasRx Alleviates
815 Symptoms of Neurological Disease in Mice. *Cell* **181**, 590-603.e516 (2020).
816 6. Z. Zheng, G. Li, C. Cui, F. Wang, X. Wang, Z. Xu, H. Guo, Y. Chen, H. Tang, D.
817 Wang, M. Huang, Z.-Y. Chen, X. Huang, H. Li, G.-L. Li, X. Hu, Y. Shu, Preventing
818 autosomal-dominant hearing loss in Bth mice with CRISPR/CasRx-based RNA
819 editing. *Signal Transduction and Targeted Therapy* **7**, 79 (2022).
820 7. J. E. Powell, C. K. W. Lim, R. Krishnan, T. X. McCallister, C. Saporito-Magriña, M.
821 A. Zeballos, G. D. McPheron, T. Gaj, Targeted gene silencing in the nervous system
822 with CRISPR-Cas13. *Science Advances* **8**, eabk2485 (2022).
823 8. Y. Li, J. Xu, X. Guo, Z. Li, L. Cao, S. Liu, Y. Guo, G. Wang, Y. Luo, Z. Zhang, X.
824 Wei, Y. Zhao, T. Liu, X. Wang, H. Xia, M. Kuang, Q. Guo, J. Li, L. Chen, Y. Wang,
825 Q. Li, F. Wang, Q. Liu, F. You, Collateral cleavage of 28s rRNA by RfxCas13d
826 causes death of mice. *bioRxiv*, 2022.2001.2017.476700 (2022).
827 9. P. Shi, M. R. Murphy, A. O. Aparicio, J. S. Kesner, Z. Fang, Z. Chen, A. Trehan, X.
828 Wu, RNA-guided cell targeting with CRISPR/RfxCas13d collateral activity in human
829 cells. *bioRxiv*, 2021.2011.2030.470032 (2021).
830 10. J. F. Bot, J. van der Oost, N. Geijsen, The double life of CRISPR–Cas13. *Current*
831 *Opinion in Biotechnology* **78**, 102789 (2022).
832 11. C. Xu, Y. Zhou, Q. Xiao, B. He, G. Geng, Z. Wang, B. Cao, X. Dong, W. Bai, Y.
833 Wang, X. Wang, D. Zhou, T. Yuan, X. Huo, J. Lai, H. Yang, Programmable RNA
834 editing with compact CRISPR–Cas13 systems from uncultivated microbes. *Nat.*
835 *Methods* **18**, 499–506 (2021).

12. S. Kannan, H. Altae-Tran, X. Jin, V. J. Madigan, R. Oshiro, K. S. Makarova, E. V. Koonin, F. Zhang, Compact RNA editors with small Cas13 proteins. *Nature Biotechnology*, 1-4 (2021).
13. H. Tong, J. Huang, Q. Xiao, B. He, X. Dong, Y. Liu, X. Yang, D. Han, Z. Wang, X. Wang, W. Ying, R. Zhang, Y. Wei, C. Xu, Y. Zhou, Y. Li, M. Cai, Q. Wang, M. Xue, G. Li, K. Fang, H. Zhang, H. Yang, High-fidelity Cas13 variants for targeted RNA degradation with minimal collateral effects. *Nature Biotechnology*, (2022).
14. G. Li, M. Jin, Z. Li, Q. Xiao, J. Lin, D. Yang, Y. Liu, X. Wang, L. Xie, W. Ying, H. Wang, E. Zuo, L. Shi, N. Wang, W. Chen, C. Xu, H. Yang, Mini-dCas13X–mediated RNA editing restores dystrophin expression in a humanized mouse model of Duchenne muscular dystrophy. *The Journal of Clinical Investigation* **133**, (2023).
15. Q. Xiao, Z. Xu, Y. Xue, C. Xu, L. Han, Y. Liu, F. Wang, R. Zhang, S. Han, X. Wang, G.-L. Li, H. Li, H. Yang, Y. Shu, Rescue of autosomal dominant hearing loss by in vivo delivery of mini dCas13X-derived RNA base editor. *Sci. Transl. Med.* **14**, eabn0449 (2022).
16. X. Deng, E. Osikpa, J. Yang, S. J. Oladeji, J. Smith, X. Gao, Y. Gao, Structural basis for the activation of a compact CRISPR-Cas13 nuclease. *Nature Communications* **14**, 5845 (2023).
17. F.-L. Lin, P.-Y. Wang, Y.-F. Chuang, J.-H. Wang, V. H. Y. Wong, B. V. Bui, G.-S. Liu, Gene Therapy Intervention in Neovascular Eye Disease: A Recent Update. *Mol. Ther.* **28**, 2120-2138 (2020).
18. M. Xu, R. Fan, X. Fan, Y. Shao, X. Li, Progress and Challenges of Anti-VEGF Agents and Their Sustained-Release Strategies for Retinal Angiogenesis. *Drug Des Devel Ther* **16**, 3241-3262 (2022).
19. Y.-F. Chuang, P.-Y. Wang, S. Kumar, S. Lama, F.-L. Lin, G.-S. Liu, Methods for in vitro CRISPR/CasRx-Mediated RNA Editing. *Frontiers in Cell and Developmental Biology* **9**, (2021).
20. Z. Li, Z. Li, X. Cheng, S. Wang, X. Wang, S. Ma, Z. Lu, H. Zhang, W. Zhao, Z. Chen, Y. Yao, C. Zhang, L. Chao, W. Li, T. Fei, Intrinsic targeting of host RNA by Cas13 constrains its utility. *Nature Biomedical Engineering*, (2023).
21. Y. Li, J. Xu, X. Guo, Z. Li, L. Cao, S. Liu, Y. Guo, G. Wang, Y. Luo, Z. Zhang, X. Wei, Y. Zhao, T. Liu, X. Wang, H. Xia, M. Kuang, Q. Guo, J. Li, L. Chen, Y. Wang, Q. Li, F. Wang, Q. Liu, F. You, The collateral activity of RfxCas13d can induce lethality in a RfxCas13d knock-in mouse model. *Genome Biol.* **24**, 20 (2023).
22. K. Ofer, B. L. Benjamin, R. S. D. Owen, J. W. t. V. Aartjan, M. Cameron, RNA structure modulates Cas13 activity and enables mismatch detection. *bioRxiv*, 2023.2010.2005.560533 (2023).
23. M. A. Lancaster, J. A. Knoblich, Organogenesis in a dish: Modeling development and disease using organoid technologies. *Science* **345**, 1247125 (2014).
24. P. Wahle, G. Brancati, C. Harmel, Z. He, G. Gut, J. S. del Castillo, A. Xavier da Silveira dos Santos, Q. Yu, P. Noser, J. S. Fleck, B. Gjeta, D. Pavlinić, S. Picelli, M. Hess, G. W. Schmidt, T. T. A. Lummen, Y. Hou, P. Galliker, D. Goldblum, M. Balogh, C. S. Cowan, H. P. N. Scholl, B. Roska, M. Renner, L. Pelkmans, B. Treutlein, J. G. Camp, Multimodal spatiotemporal phenotyping of human retinal organoid development. *Nature Biotechnology*, (2023).
25. V. I. Maryna, M. H. Daniel, M. M. Eric, T. B. Kevin, W. Mantian, W. P. Cole, J. K. Alex, C. Xinlan, L. Yaqiao, G. Bence, P. C. David, PCDH15 Dual-AAV Gene

883 Therapy for Deafness and Blindness in Usher Syndrome Type 1F. *bioRxiv*,
884 2023.2011.2009.566447 (2023).
885 26. E. L. West, P. Majumder, A. Naeem, M. Fernando, M. O'Hara-Wright, E. Lanning,
886 M. Kloc, J. Ribeiro, P. Ovando-Roche, I. O. Shum, N. Jumbu, R. Sampson, M. Hayes,
887 J. W. B. Bainbridge, A. Georgiadis, A. J. Smith, A. Gonzalez-Cordero, R. R. Ali,
888 Antioxidant and lipid supplementation improve the development of photoreceptor
889 outer segments in pluripotent stem cell-derived retinal organoids. *Stem Cell Reports*
890 **17**, 775-788 (2022).
891 27. H. J. Kim, M. O'Hara-Wright, D. Kim, T. H. Loi, B. Y. Lim, R. V. Jamieson, A.
892 Gonzalez-Cordero, P. Yang, Comprehensive characterization of fetal and mature
893 retinal cell identity to assess the fidelity of retinal organoids. *Stem Cell Reports* **18**,
894 175-189 (2023).
895 28. H. Hu, S.-C. Sun, Ubiquitin signaling in immune responses. *Cell Research* **26**, 457-
896 483 (2016).
897 29. E. P. Rakoczy, I. S. Ali Rahman, N. Binz, C.-R. Li, N. N. Vagaja, M. de Pinho, C.-M.
898 Lai, Characterization of a mouse model of hyperglycemia and retinal
899 neovascularization. *Am J Pathol* **177**, 2659-2670 (2010).
900 30. R. Nakagawa, S. Kannan, H. Altae-Tran, S. N. Takeda, A. Tomita, H. Hirano, T.
901 Kusakizako, T. Nishizawa, K. Yamashita, F. Zhang, H. Nishimasu, O. Nureki,
902 Structure and engineering of the minimal type VI CRISPR-Cas13bt3. *Molecular Cell*
903 **82**, 3178-3192.e3175 (2022).
904 31. K. Nishijima, Y.-S. Ng, L. Zhong, J. Bradley, W. Schubert, N. Jo, J. Akita, S. J.
905 Samuelsson, G. S. Robinson, A. P. Adamis, D. T. Shima, Vascular Endothelial
906 Growth Factor-A Is a Survival Factor for Retinal Neurons and a Critical
907 Neuroprotectant during the Adaptive Response to Ischemic Injury. *Am J Pathol* **171**,
908 53-67 (2007).
909 32. Y.-Z. Le, VEGF production and signaling in Müller glia are critical to modulating
910 vascular function and neuronal integrity in diabetic retinopathy and hypoxic retinal
911 vascular diseases. *Vision Research* **139**, 108-114 (2017).
912 33. K. M. Ford, M. Saint-Geniez, T. Walshe, A. Zahr, P. A. D'Amore, Expression and
913 Role of VEGF in the Adult Retinal Pigment Epithelium. *Investigative Ophthalmology*
914 *& Visual Science* **52**, 9478-9487 (2011).
915 34. D. Colognori, M. Trinidad, J. A. Doudna, Precise transcript targeting by CRISPR-
916 Csm complexes. *Nature Biotechnology* **41**, 1256-1264 (2023).
917 35. N. Jo, C. Mailhos, M. Ju, E. Cheung, J. Bradley, K. Nishijima, G. S. Robinson, A. P.
918 Adamis, D. T. Shima, Inhibition of Platelet-Derived Growth Factor B Signaling
919 Enhances the Efficacy of Anti-Vascular Endothelial Growth Factor Therapy in
920 Multiple Models of Ocular Neovascularization. *Am J Pathol* **168**, 2036-2053 (2006).
921 36. J. Park, G. Cui, H. Lee, H. Jeong, J. J. Kwak, J. Lee, S. H. Byeon, CRISPR/Cas9
922 mediated specific ablation of vegfa in retinal pigment epithelium efficiently regresses
923 choroidal neovascularization. *Sci. Rep.* **13**, 3715 (2023).
924 37. M. Garita-Hernandez, F. Routet, L. Guibbal, H. Khabou, L. Toualbi, L. Riancho, S.
925 Reichman, J. Duebel, J. A. Sahel, O. Goureau, D. Dalkara, AAV-Mediated Gene
926 Delivery to 3D Retinal Organoids Derived from Human Induced Pluripotent Stem
927 Cells. *Int J Mol Sci* **21**, (2020).
928 38. M. E. McClements, H. Steward, W. Atkin, E. A. Goode, C. Gándara, V. Chichagova,
929 R. E. MacLaren, Tropism of AAV Vectors in Photoreceptor-Like Cells of Human

930 iPSC-Derived Retinal Organoids. *Translational Vision Science & Technology* **11**, 3-3
931 (2022).
932 39. T. T. Duong, J. Lim, V. Vasireddy, T. Papp, H. Nguyen, L. Leo, J. Pan, S. Zhou, H. I.
933 Chen, J. Bennett, J. A. Mills, Comparative AAV-eGFP Transgene Expression Using
934 Vector Serotypes 1–9, 7m8, and 8b in Human Pluripotent Stem Cells, RPEs, and
935 Human and Rat Cortical Neurons. *Stem Cells International* **2019**, 7281912 (2019).
936 40. S. Eoi Jong, A. C. Jeong, K. Jae-Young, Y. Young Hee, Aflibercept ameliorates
937 retinal pericyte loss and restores perfusion in streptozotocin-induced diabetic mice.
938 *BMJ Open Diabetes Research & Care* **8**, e001278 (2020).
939 41. C. C. Tokunaga, K. P. Mitton, W. Dailey, C. Massoll, K. Roumayah, E. Guzman, N.
940 Tarabishy, M. Cheng, K. A. Drenser, Effects of Anti-VEGF Treatment on the
941 Recovery of the Developing Retina Following Oxygen-Induced Retinopathy.
942 *Investigative Ophthalmology & Visual Science* **55**, 1884-1892 (2014).
943 42. C. P. Shah, S. J. Garg, J. F. Vander, G. C. Brown, R. S. Kaiser, J. A. Haller,
944 Outcomes and Risk Factors Associated with Endophthalmitis after Intravitreal
945 Injection of Anti-Vascular Endothelial Growth Factor Agents. *Ophthalmology* **118**,
946 2028-2034 (2011).
947 43. A. K. W. Lai, A. C. Y. Lo, Animal Models of Diabetic Retinopathy: Summary and
948 Comparison. *Journal of Diabetes Research* **2013**, 106594 (2013).
949 44. L. E. H. Smith, W. Shen, C. Perruzzi, S. Soker, F. Kinose, X. Xu, G. Robinson, S.
950 Driver, J. Bischoff, B. Zhang, J. M. Schaeffer, D. R. Senger, Regulation of vascular
951 endothelial growth factor-dependent retinal neovascularization by insulin-like growth
952 factor-1 receptor. *Nat. Med.* **5**, 1390-1395 (1999).
953 45. X. Huang, G. Zhou, W. Wu, Y. Duan, G. Ma, J. Song, R. Xiao, L. Vandenberghe, F.
954 Zhang, P. A. D'Amore, H. Lei, Genome editing abrogates angiogenesis in vivo.
955 *Nature Communications* **8**, 112 (2017).
956 46. A. Holmgaard, A. L. Askou, J. N. E. Benckendorff, E. A. Thomsen, Y. Cai, T. Bek, J.
957 G. Mikkelsen, T. J. Corydon, In Vivo Knockout of the Vegfa Gene by Lentiviral
958 Delivery of CRISPR/Cas9 in Mouse Retinal Pigment Epithelium Cells. *Molecular*
959 *Therapy - Nucleic Acids* **9**, 89-99 (2017).
960 47. A. B. Holmgaard, A. L. Askou, E. G. Jensen, S. Alsing, R. O. Bak, J. G. Mikkelsen,
961 T. J. Corydon, Targeted Knockout of the Vegfa Gene in the Retina by
962 Subretinal Injection of RNP Complexes Containing Cas9 Protein and Modified
963 sgRNAs. *Mol. Ther.* **29**, 191-207 (2021).
964 48. Y. Wang, B. Wang, H. Xie, Q. Ren, X. Liu, F. Li, X. Lv, X. He, C. Cheng, R. Deng,
965 J. Li, J. Zhao, Z. Song, F. Gu, Efficient Human Genome Editing Using SaCas9
966 Ribonucleoprotein Complexes. *Biotechnology journal* **14**, e1800689 (2019).
967 49. S. H. Chung, T.-N. Sin, B. Dang, T. Ngo, T. Lo, D. Lent-Schochet, R. K. Meleppat,
968 R. J. Zawadzki, G. Yiu, CRISPR-based VEGF suppression using paired guide RNAs
969 for treatment of choroidal neovascularization. *Molecular Therapy - Nucleic Acids* **28**,
970 613-622 (2022).
971 50. S. Konermann, P. Lotfy, N. J. Brideau, J. Oki, M. N. Shokhirev, P. D. Hsu,
972 Transcriptome Engineering with RNA-Targeting Type VI-D CRISPR Effectors. *Cell*
973 **173**, 665-676.e614 (2018).
974 51. C.-M. Lai, Generation of transgenic mice with mild and severe retinal
975 neovascularisation. *Br J Ophthalmol* **89**, 911-916 (2005).
976 52. E. Zudaire, L. Gambardella, C. Kurcz, S. Vermeren, A Computational Tool for
977 Quantitative Analysis of Vascular Networks. *PLoS One* **6**, e27385 (2011).

53. S. Andrews. (Babraham Bioinformatics, Babraham Institute, Cambridge, United Kingdom, 2010).
54. A. M. Bolger, M. Lohse, B. Usadel, Trimmomatic: a flexible trimmer for Illumina sequence data. *Bioinformatics* **30**, 2114-2120 (2014).
55. A. Dobin, C. A. Davis, F. Schlesinger, J. Drenkow, C. Zaleski, S. Jha, P. Batut, M. Chaisson, T. R. Gingeras, STAR: ultrafast universal RNA-seq aligner. *Bioinformatics* **29**, 15-21 (2013).
56. B. Li, C. N. Dewey, RSEM: accurate transcript quantification from RNA-Seq data with or without a reference genome. *BMC bioinformatics* **12**, 1-16 (2011).
57. J.-H. Hung, T.-H. Yang, Z. Hu, Z. Weng, C. DeLisi, Gene set enrichment analysis: performance evaluation and usage guidelines. *Briefings in bioinformatics* **13**, 281-291 (2012).
58. G. O. Consortium, The Gene Ontology (GO) database and informatics resource. *Nucleic acids research* **32**, D258-D261 (2004).
59. G. Yu, L.-G. Wang, Y. Han, Q.-Y. He, clusterProfiler: an R package for comparing biological themes among gene clusters. *Omics: a journal of integrative biology* **16**, 284-287 (2012).
60. A. Gordon, G. J. Hannon, Fastx-toolkit. *FASTQ/A short-reads preprocessing tools (unpublished) http://hannonlab. cshl. edu/fastx_toolkit* **5**, (2010).
61. J. Ye, S. McGinnis, T. L. Madden, BLAST: improvements for better sequence analysis. *Nucleic acids research* **34**, W6-W9 (2006).
62. A. Ianevski, A. K. Giri, T. Aittokallio, Fully-automated and ultra-fast cell-type identification using specific marker combinations from single-cell transcriptomic data. *Nature communications* **13**, 1246 (2022).
63. G. A. Limb, T. E. Salt, P. M. Munro, S. E. Moss, P. T. Khaw, In vitro characterization of a spontaneously immortalized human Müller cell line (MIO-M1). *Invest Ophthalmol Vis Sci* **43**, 864-869 (2002).
64. M. I. Love, W. Huber, S. Anders, Moderated estimation of fold change and dispersion for RNA-seq data with DESeq2. *Genome Biol.* **15**, 550 (2014).
65. Y. Hao, T. Stuart, M. H. Kowalski, S. Choudhary, P. Hoffman, A. Hartman, A. Srivastava, G. Molla, S. Madad, C. Fernandez-Granda, R. Satija, Dictionary learning for integrative, multimodal and scalable single-cell analysis. *Nature Biotechnology*, (2023).

Acknowledgments

The authors would like to thank MAnusha H Shah, Liuhui Huang, Jesse Gardner-Russell and Yujie Wang for their assistance with retinal dissections, Prof Alex Hewitt and Dr Leilei Tu for providing resources for vector construction. The authors also extend their gratitude to the Vector and Genome Engineering Facility (VGEF) and the Single Cell Analytics Facility at the Children's Medical Research Institute (CMRI) for producing AAV vectors and the scRNA-seq

experiments respectively and Azenta Life Sciences for conducting RNA sequencing. Schematic in figures were designed using Biorender.com.

Funding: This work was supported by grants from the National Health and Medical Research Council of Australia (NHMRC; GNT1185600), CERA Innovation Fund, National Natural Science Foundation of China (No. 82201227), and Natural Science Foundation of Guangdong Province, China (No. 2023A1515011225). Anai Gonzalez Cordero is an Al & Val Rosenstrauss Fellow (Rebecca Cooper Foundation). Funds supporting this work included the Medical Research Future Fund Stem Cell Mission (MRFF; MRF2008912), and the National Stem Cell Foundation - Metcalf Award Prize (No 00339). Satheesh Kumar was supported by the Melbourne Research Scholarship and Graeme Clark Institute Top-Up Scholarship. The Centre for Eye Research Australia receives Operational Infrastructure Support from the Victorian Government.

Author contributions:

Conceptualization: SK, GSL. Methodology: SK, YWH, VHYW, DA, LAM, AGC, BVB, GSL. Investigation: SK, YWH, VHYW, DA, AGC, BVB, GSL. Validation: SK, YWH, GSL. Formal analysis: SK, YWH, GSL. Data curation: SK, YWH, GSL. Visualization: SK, YWH, DA, AGC, GSL. Resources: LAM, AGC, BVB, GSL. Supervision: GSL. Writing—original draft: SK, GSL. Writing—review & editing: SK, YWH, AGC, BVB, GSL. Project administration: GSL. Funding acquisition: AGC, GSL

Competing interests: The authors declare that they have no known competing financial interests.

Data and materials availability: RNA sequencing data generated from this study is available under the GEO accession numbers: GSE259219 and GSE259220. All data are available in the main text or the supplementary materials. Other data generated and/or analysed in this current study will be available from the corresponding author upon reasonable request.

1048 **Supplementary Materials**

1049

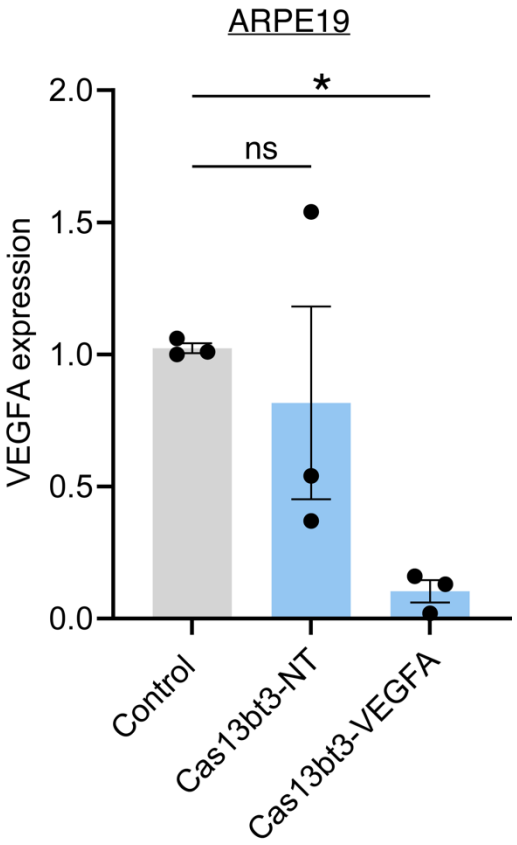

1050

1051 **Figure S1. Evaluation of Cas13bt3 targeting in retinal cell lines.** VEGFA mRNA expression
1052 in ARPE19 cells following transfection of control, Cas13bt3-NT and Cas13bt3-VEGFA. A
1053 significant reduction in Cas13bt3-VEGFA was observed. Data presented as mean ± SEM. ns:
1054 not significant. *P≤0.05.

1055

1056

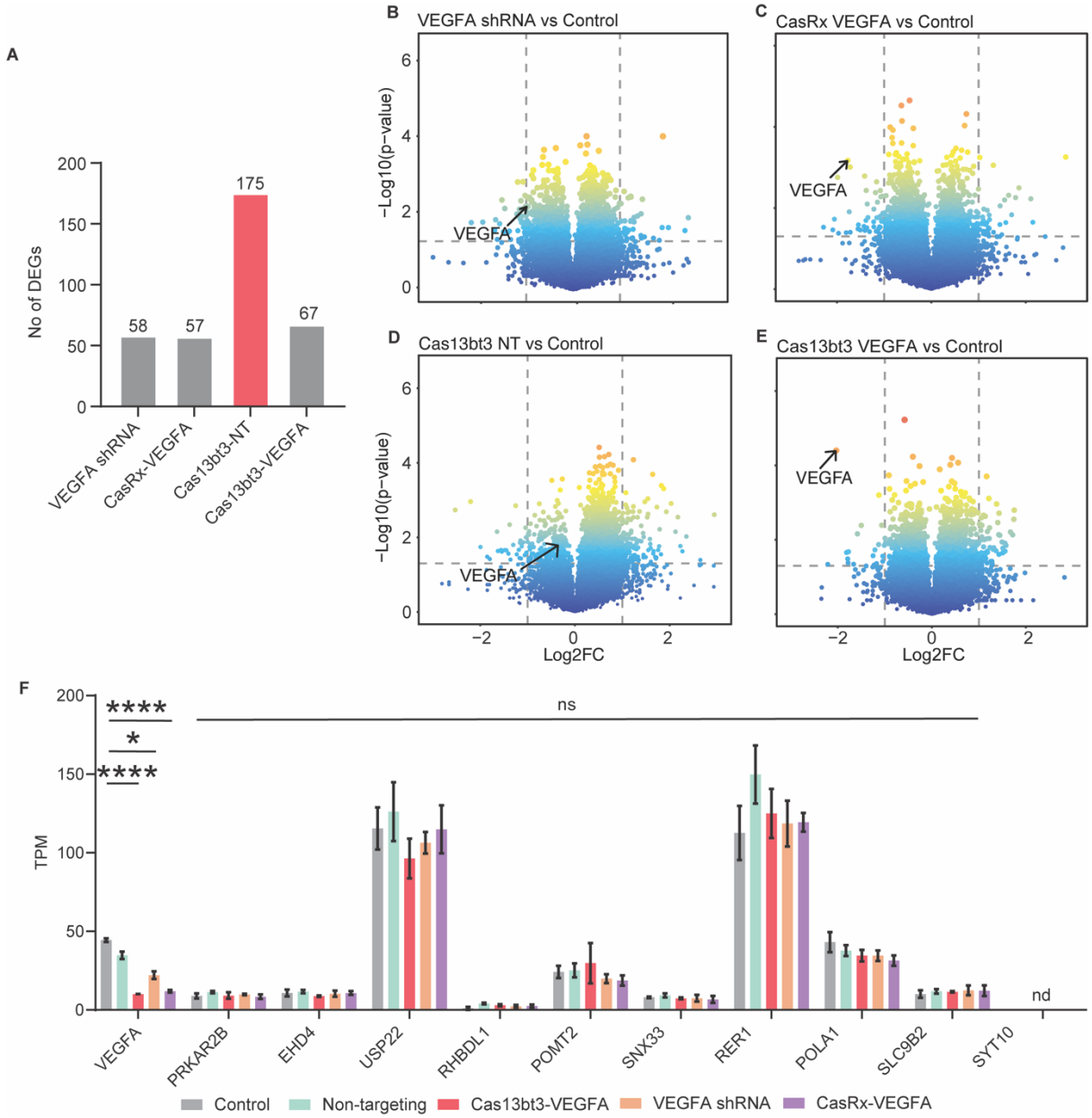
A
No of DEGs
200
150
100
50
0
58
57
175
67
VEGFA shRNA
CasRx-VEGFA
Cas13bt3-NT
Cas13bt3-VEGFA
B
VEGFA shRNA vs Control
C
CasRx VEGFA vs Control
D
Cas13bt3 NT vs Control
E
Cas13bt3 VEGFA vs Control
−Log10(p−value)
VEGFA
Log2FC
F
TPM
****
*
****
ns
nd
VEGFA
PRKAR2B
EHD4
USP22
RHBDL1
POMT2
SNX33
RER1
POLA1
SLC9B2
SYT10
Control
Non-targeting
Cas13bt3-VEGFA
VEGFA shRNA
CasRx-VEGFA

1057

1058 **Figure S2. HEK293FT DEG and off target analysis. (A)** Number of differentially expressed
1059 genes from the VEGFA-targeting shRNA, CasRx and Cas13bt3 transfections in HEK293FT
1060 cells compared to vector control. **(B)** Volcano plots of differentially expressed genes from
1061 VEGFA shRNA, **(C)** CasRx VEGFA sgRNA, **(D)** Cas13bt3 NT sgRNA and **(E)** Cas13bt3
1062 VEGFA sgRNA compared to vector control. **(F)** Plot of TPM values for VEGFA and candidate
1063 off-target genes from Cas13bt3-NT sgRNA and Cas13bt3 VEGFA sgRNA groups compared
1064 to shRNA and CasRx targeting vectors. Statistical analysis was conducted by Welch's t test
1065 **(F)**. Data presented as mean ± SEM. ns: not significant. *P≤0.05, ****P≤0.00001.

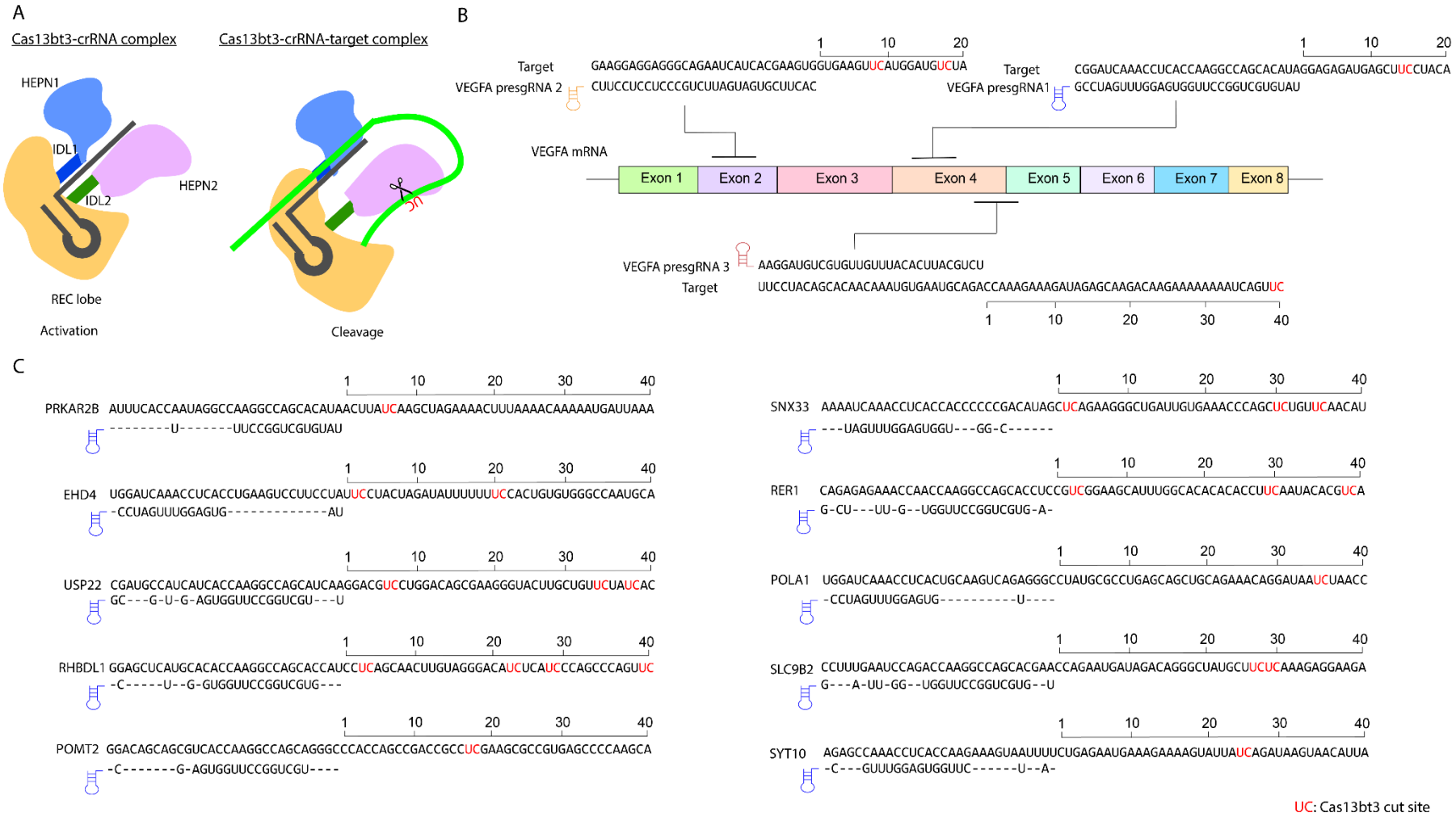
A
Cas13bt3-crRNA complex
Cas13bt3-crRNA-target complex
HEPN1
IDL1
IDL2
HEPN2
REC lobe
Activation
Cleavage
B
Target
GAAGGAGGAGGGCAGAAUCAUCACGAAGUGGUGAAGUUCAUGGAUGUCUA
VEGFA presgRNA 2
CUUCCUCCUCCCGUCUUAGUAGUGCUUCAC
Target
CGGAUCAAACCUCACCAAGGCCAGCACAUAGGAGAGAUGAGCUUCCUACA
VEGFA presgRNA1
GCCUAGUUUGGAGUGGUUCCGGUCGUGUAU
VEGFA mRNA
Exon 1
Exon 2
Exon 3
Exon 4
Exon 5
Exon 6
Exon 7
Exon 8
VEGFA presgRNA 3
AAGGAUGUCGUGUUGUUUACACUUACGUCU
Target
UUCCUACAGCACAACAAAUGUGAAUGCAGACCAAAGAAAGAUAGAGCAAGACAAGAAAAAAAAUCAGUUC
C
PRKAR2B AUUUCACCAAUAGGCCAAGGCCAGCACAUAACUUAUCAAGCUAGAAAACUUUAAAACAAAAAUGAUUAAA
--------U-------UUCCGGUCGUGUAU
EHD4 UGGAUCAAACCUCACCUGAAGUCCUUCCUAUUCCUACUAGAUAUUUUUUCCACUGUGUGGGCCAAUGCA
-CCUAGUUUGGAGUG----------AU
USP22 CGAUGCCAUCAUCACCAAGGCCAGCAUCAAGGACGUCCUGGACAGCGAAGGGUACUUGCUGUUCUAUCAC
GC---G-U-G-AGUGGUUCCGGUCGU---U
RHBDL1 GGAGCUCAUGCACACCAAGGCCAGCACCAUCCUCAGCAACUUGUAGGGACAUCUCAUCCCAGCCCAGUUC
-C-----U--G-GUGGUUCCGGUCGUG---
POMT2 GGACAGCAGCGUCACCAAGGCCAGCAGGGCCCACCAGCCGACCGCCUCGAAGCGCCGUGAGCCCCAAGCA
-C-------G-AGUGGUUCCGGUCGU----
SNX33 AAAAUCAAACCUCACCACCCCCCGACAUAGCUCAGAAGGGCUGAUUGUGAAACCCAGCUCUGUUCAACAU
---UAGUUUGGAGUGGU---GG-C------
RER1 CAGAGAGAAACCAACCAAGGCCAGCACCUCCGUCGGAAGCAUUUGGCACACACACCUUCAAUACACGUCA
G-CU---UU-G--UGGUUCCGGUCGUG-A-
POLA1 UGGAUCAAACCUCACUGCAAGUCAGAGGGCCUAUGCGCCUGAGCAGCUGCAGAAACAGGAUAAUCUAACC
-CCUAGUUUGGAGUG----------U----
SLC9B2 CCUUUGAAUCCAGACCAAGGCCAGCACGAACCAGAAUGAUAGACAGGGCUAUGCUUCUCAAAGAGGAAGA
G---A-UU-GG--UGGUUCCGGUCGUG--U
SYT10 AGAGCCAAACCUCACCAAGAAAGUAAUUUUCUGAGAAUGAAAGAAAAGUAUUAUCAGAUAAGUAACAUUA
-C---GUUUGGAGUGGUUC------U--A-
UC: Cas13bt3 cut site

1066

1067 **Figure S3. Prediction of Cas13bt3 cut sites**. **(A)** Schematic of Cas13bt3-gRNA and Cas13bt3-gRNA-target complex. **(B)** Potential Cas13bt3 cut
1068 sites on VEGFA mRNA target for VEGFA sgRNA1, 2 and 3. **(C)** Potential Cas13bt3 cut sites on top 10 candidate off-target genes for VEFGA
1069 sgRNA 1.

1070

```
A  VEGFA        TATGTGCTGGCCTTGGTGAGGTTTGATCCG
   PRKAR2B      TATGTGCTGGCCTTGG--------------
   EHD4         ---------------GGTGAGGTTTGATCC-
   USP22        ----TGCTGGCCTTGGTGA-----------
   RHBDL1       ---GTGCTGGCCTTGGTG------------
   POMT2        ----TGCTGGCCTTGGTGA-----------
   SNX33        --------------TGGTGAGGTTTGAT---
   RER1         ---GTGCTGGCCTTGGT-------------
   POLA1        ----------------GTGAGGTTTGATCC-
   SLC9B2       ---GTGCTGGCCTTGGT-------------
   SYT10        -----------CTTGGTGAGGTTTG-----

B  VEGFA presgRNA 2  CACTTCGTGATGATTCTGCCCTCCTCCTTC
   BARX1        ---------------TCTGCCCTCCTCCTTC
   SLX4         ---------------TCTGCCCTCCTCCTTC
   LOC 100192426 ---------------TCTGCCCTCCTCCTTC
   NRG1         --------GATGATTCTGCCCTC-------
   AGRN         -----------ATTCTGCCCTCCTCC---
   TRIM56       ---------------CTGCCCTCCTCCTTC
   CDH20        -----------GATTCTGCCCTCCTCCTTC
   MORC3        ----------TGATTCTGCCCTCCT-----
   ZNF32-AS3    ---------------CTGCCCTCCTCCTTC
   SUGT1P4-STRA6LP  CACTTCGTGATGAT----------------

C  VEGFA presgRNA 3  TCTGCATTCACATTTGTTGTGCTGTAGGAA
   NUP210L      ----------CATTTGTTGTGCTGT-----
   LOC 105373744  TCTGCATTCACATTT---------------
   LYSMD3       ----------CATTTGTTGTGCTGT-----
   SKP1         -CTGCATTCACATTTG--------------
   CPA4         --TGCATTCACATTTG--------------
   SENP5        -CTGCATTCACATTTGTT------------
```

1073 **Figure S4. Multiplexed VEGFA knockdown using Cas13bt3. (A)** Top off-target genes for
1074 VEGFA sgRNA 1, **(B)** VEGFA sgRNA 2 and **(C)** VEGFA sgRNA 3.

1075

1076

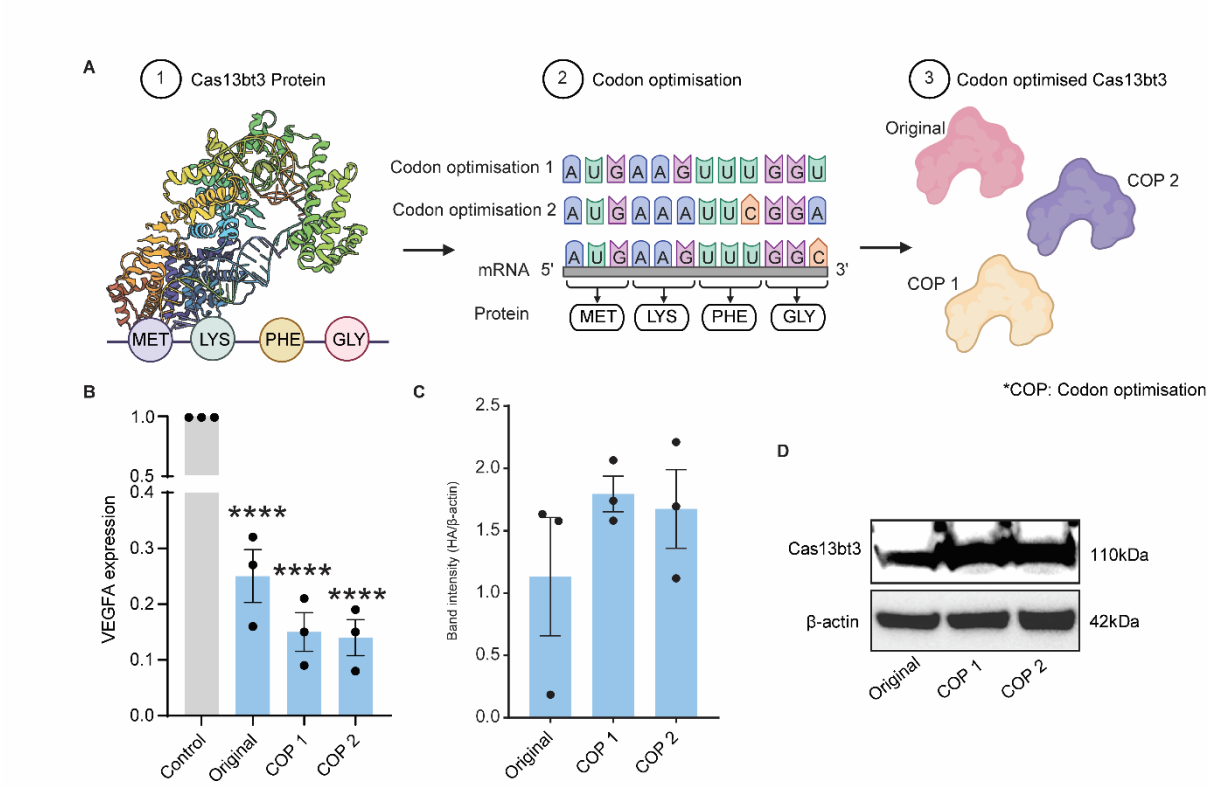
A
1 Cas13bt3 Protein
2 Codon optimisation
3 Codon optimised Cas13bt3
Codon optimisation 1
Codon optimisation 2
mRNA 5'
3'
Protein
MET
LYS
PHE
GLY
Original
COP 2
COP 1
*COP: Codon optimisation
B
VEGFA expression
Control
Original
COP 1
COP 2
C
Band intensity (HA/β-actin)
D
Cas13bt3
110kDa
β-actin
42kDa

1077

1078 **Figure S5. Codon optimisation of Cas13bt3. (A)** Schematic of codon optimisation procedure
1079 from Cas13e protein sequence. **(B)** VEGFA mRNA knockdown from original and codon
1080 optimised Cas13e compared to control transfection. **(C and D)** Expression of original and
1081 codon optimised determined from Western blot. Statistical analyses was conducted using One-
1082 way ANOVA with Tukey's multiple comparisons test (**B and C**). Data presented as mean ±
1083 SEM. *P≤0.05, **P≤0.001, ****P≤0.00001.

1084

1085

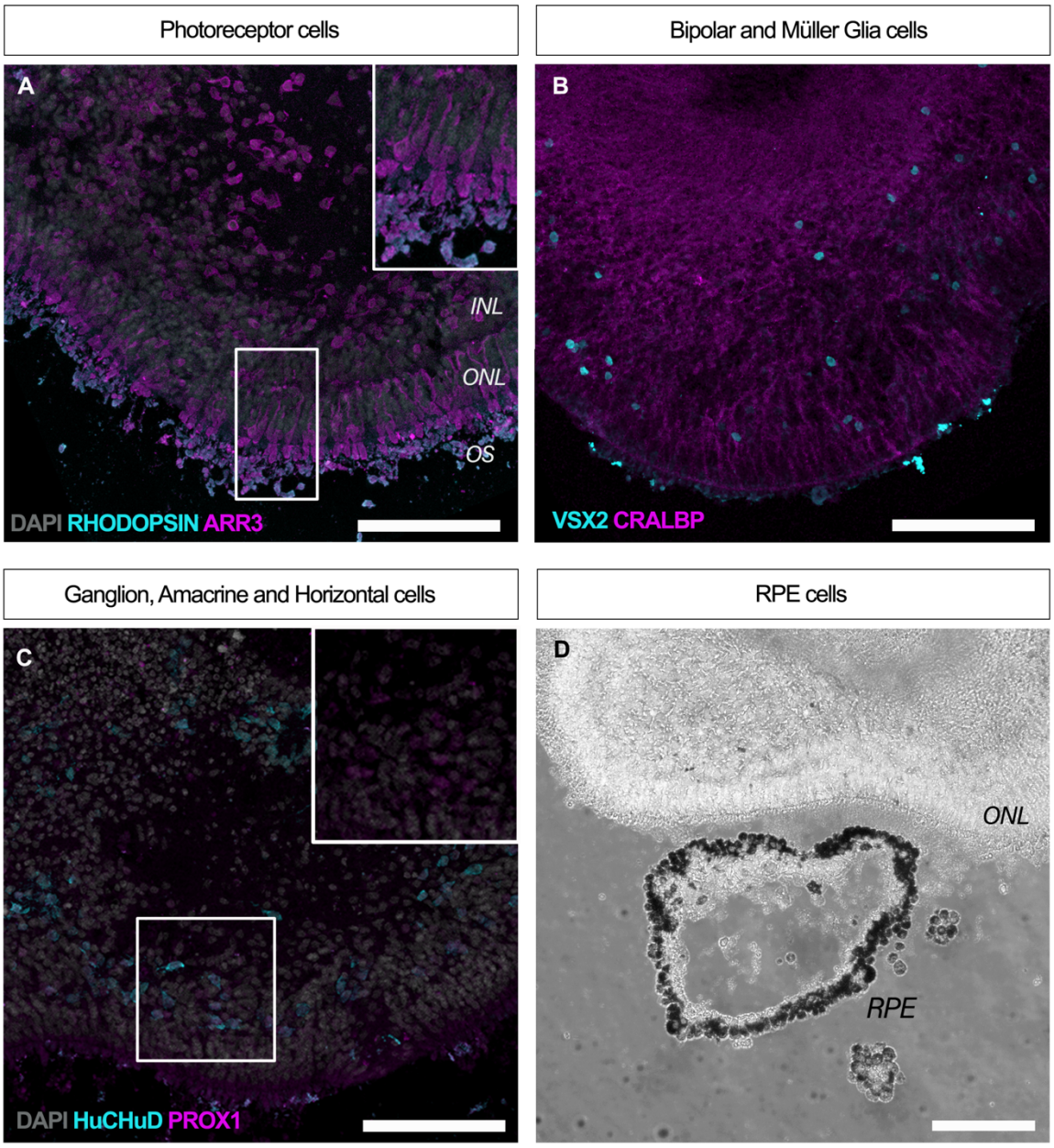
Photoreceptor cells
Bipolar and Müller Glia cells
A
INL
ONL
OS
DAPI RHODOPSIN ARR3
B
VSX2 CRALBP
Ganglion, Amacrine and Horizontal cells
RPE cells
C
DAPI HuCHuD PROX1
D
ONL
RPE

1086

1087 **Figure S6. Characterization of 30 weeks retinal organoids. (A)** Retinal organoids showed
1088 expression of mature photoreceptor markers Arrestin-3 (magenta) specific to the cone cells and
1089 Rhodopsin (cyan) localized to the outer segments (OS) of rod photoreceptor cells. **(B, C)** In
1090 the inner nuclear layer (INL) bipolar cells stained with VSX2 (cyan) and Müller glia stained
1091 with CRALBP (magenta) **(B)**, Amacrine and horizontal cells stained with PROX1 (magenta)
1092 and ganglion cells stained with HuCHuD (cyan) **(C)**. **(D)** Brightfield image of retinal organoid
1093 section showing the outer nuclear layer (ONL) and a pigmented RPE island next to it. Scale
1094 bar: 116μm. Abbreviations: INL: inner nuclear layer ONL: outer Nuclear Layer, OS: outer
1095 segment, RPE: retinal pigment epithelium.

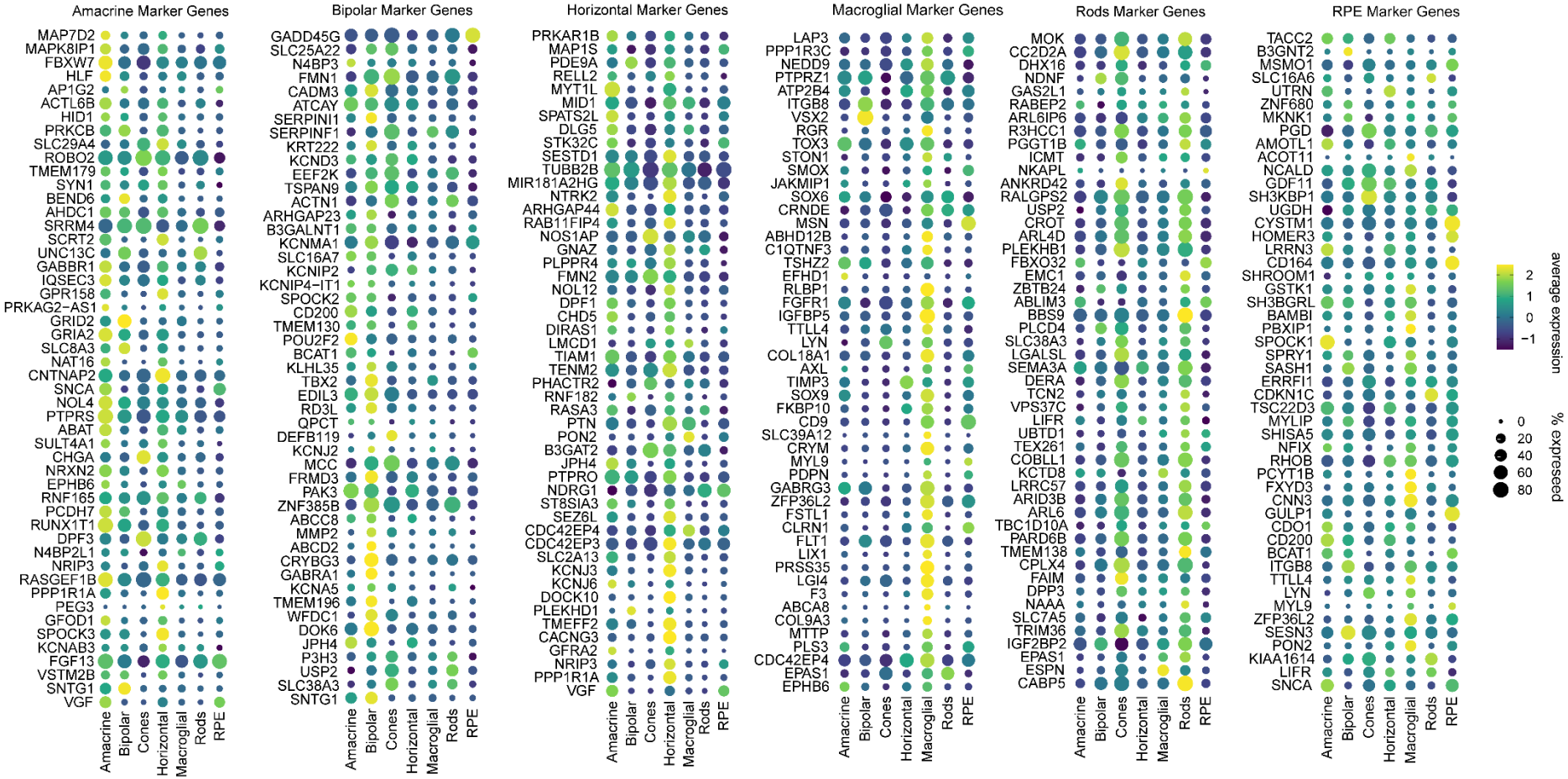
Amacrine Marker Genes
MAP7D2
MAPK8IP1
FBXW7
HLF
AP1G2
ACTL6B
HID1
PRKCB
SLC29A4
ROBO2
TMEM179
SYN1
BEND6
AHDC1
SRRM4
SCRT2
UNC13C
GABBR1
IQSEC3
GPR158
PRKAG2−AS1
GRID2
GRIA2
SLC8A3
NAT16
CNTNAP2
SNCA
NOL4
PTPRS
ABAT
SULT4A1
CHGA
NRXN2
EPHB6
RNF165
PCDH7
RUNX1T1
DPF3
N4BP2L1
NRIP3
RASGEF1B
PPP1R1A
PEG3
GFOD1
SPOCK3
KCNAB3
FGF13
VSTM2B
SNTG1
VGF
Amacrine
Bipolar
Cones
Horizontal
Macroglial
Rods
RPE
Bipolar Marker Genes
GADD45G
SLC25A22
N4BP3
FMN1
CADM3
ATCAY
SERPINI1
SERPINF1
KRT222
KCND3
EEF2K
TSPAN9
ACTN1
ARHGAP23
B3GALNT1
KCNMA1
SLC16A7
KCNIP2
KCNIP4−IT1
SPOCK2
CD200
TMEM130
POU2F2
BCAT1
KLHL35
TBX2
EDIL3
RD3L
QPCT
DEFB119
KCNJ2
MCC
FRMD3
PAK3
ZNF385B
ABCC8
MMP2
ABCD2
CRYBG3
GABRA1
KCNA5
TMEM196
WFDC1
DOK6
JPH4
P3H3
USP2
SLC38A3
SNTG1
Horizontal Marker Genes
PRKAR1B
MAP1S
PDE9A
RELL2
MYT1L
MID1
SPATS2L
DLG5
STK32C
SESTD1
TUBB2B
MIR181A2HG
NTRK2
ARHGAP44
RAB11FIP4
NOS1AP
GNAZ
PLPPR4
FMN2
NOL12
DPF1
CHD5
DIRAS1
LMCD1
TIAM1
TENM2
PHACTR2
RNF182
RASA3
PTN
PON2
B3GAT2
JPH4
PTPRO
NDRG1
ST8SIA3
SEZ6L
CDC42EP4
CDC42EP3
SLC2A13
KCNJ3
KCNJ6
DOCK10
PLEKHD1
TMEFF2
CACNG3
GFRA2
NRIP3
PPP1R1A
VGF
Macroglial Marker Genes
LAP3
PPP1R3C
NEDD9
PTPRZ1
ATP2B4
ITGB8
VSX2
RGR
TOX3
STON1
SMOX
JAKMIP1
SOX6
CRNDE
MSN
ABHD12B
C1QTNF3
TSHZ2
EFHD1
RLBP1
FGFR1
IGFBP5
TTLL4
LYN
COL18A1
AXL
TIMP3
SOX9
FKBP10
CD9
SLC39A12
CRYM
MYL9
PDPN
GABRG3
ZFP36L2
FSTL1
CLRN1
FLT1
LIX1
PRSS35
LGI4
F3
ABCA8
COL9A3
MTTP
PLS3
CDC42EP4
EPAS1
EPHB6
Rods Marker Genes
MOK
CC2D2A
DHX16
NDNF
GAS2L1
RABEP2
ARL6IP6
R3HCC1
PGGT1B
ICMT
NKAPL
ANKRD42
RALGPS2
USP2
CROT
ARL4D
PLEKHB1
FBXO32
EMC1
ZBTB24
ABLIM3
BBS9
PLCD4
SLC38A3
LGALSL
SEMA3A
DERA
TCN2
VPS37C
LIFR
UBTD1
TEX261
COBLL1
KCTD8
LRRC57
ARID3B
ARL6
TBC1D10A
PARD6B
TMEM138
CPLX4
FAIM
DPP3
NAAA
SLC7A5
TRIM36
IGF2BP2
EPAS1
ESPN
CABP5
RPE Marker Genes
TACC2
B3GNT2
MSMO1
SLC16A6
UTRN
ZNF680
MKNK1
PGD
AMOTL1
ACOT11
NCALD
GDF11
SH3KBP1
UGDH
CYSTM1
HOMER3
LRRN3
CD164
SHROOM1
GSTK1
SH3BGRL
BAMBI
PBXIP1
SPOCK1
SPRY1
SASH1
ERRFI1
CDKN1C
TSC22D3
MYLIP
SHISA5
NFIX
RHOB
PCYT1B
FXYD3
CNN3
GULP1
CDO1
CD200
BCAT1
ITGB8
TTLL4
LYN
MYL9
ZFP36L2
SESN3
PON2
KIAA1614
LIFR
SNCA
average expression
2
1
0
−1
% expressed
0
20
40
60
80

1096

1097

1098 **Figure S7. Dot plots of retinal cell marker genes for respective cell types in 3D retinal organoids.** Complete list of cell marker genes can
1099 obtained from Kim et al., 2023 (*27*).

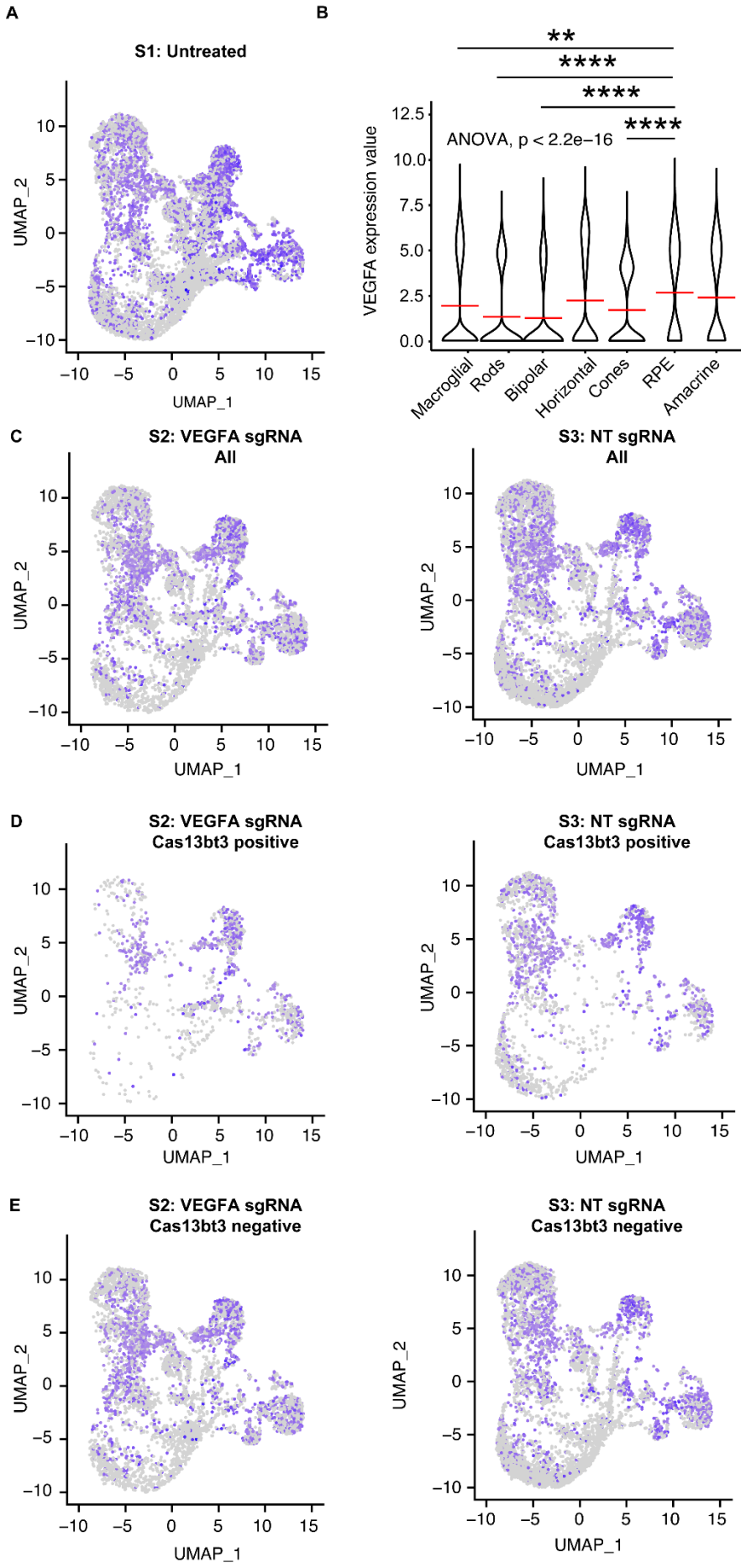
A
S1: Untreated
UMAP_2
UMAP_1
B
**
****
****
****
ANOVA, p < 2.2e−16
VEGFA expression value
Macroglial
Rods
Bipolar
Horizontal
Cones
RPE
Amacrine
C
S2: VEGFA sgRNA
All
S3: NT sgRNA
All
D
S2: VEGFA sgRNA
Cas13bt3 positive
S3: NT sgRNA
Cas13bt3 positive
E
S2: VEGFA sgRNA
Cas13bt3 negative
S3: NT sgRNA
Cas13bt3 negative

1101 **Figure S8. *E*xpression of VEGFA *on* retinal cell clusters.** UMAP plots of showing
1102 expression on **(A)** Untreated retinal organoid. **(B)** Violin plots showing expression of VEGFA
1103 in individual retinal cell types. **(C)** UMAP plots of retinal cell clusters with expression of
1104 VEGFA from VEGFA-treated and NT-treated retinal organoids, all cells, **(D)** Cas13bt3
1105 positive cells and **(E)** Cas13bt3 negative cells. Data analyses were conducted using One-way
1106 ANOVA with Tukey's multiple comparisons test (B). **P≤0.001, ****P≤0.00001.

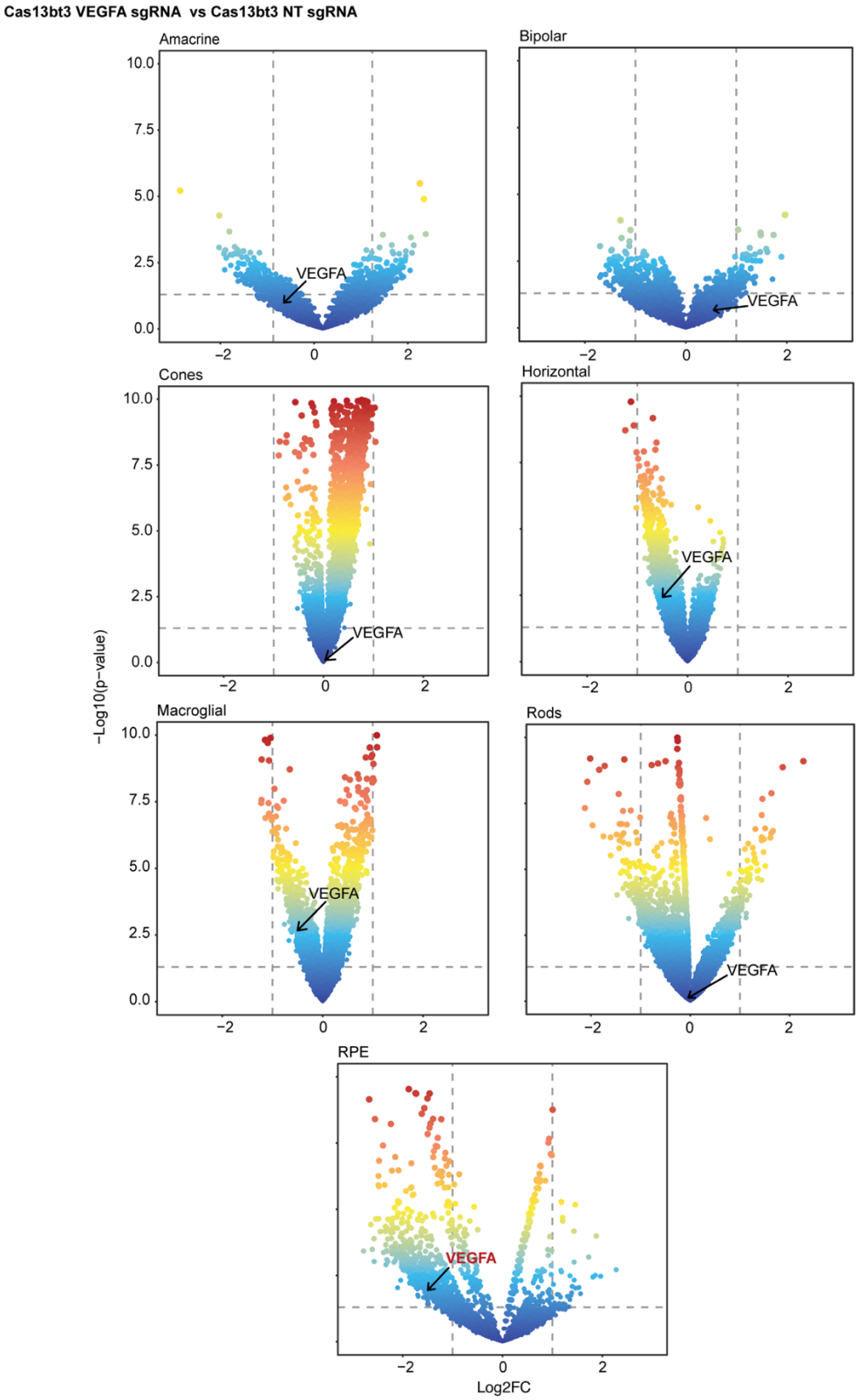
Cas13bt3 VEGFA sgRNA vs Cas13bt3 NT sgRNA
Amacrine
Bipolar
Cones
Horizontal
Macroglial
Rods
RPE
VEGFA
−Log10(p−value)
Log2FC

1107

1108

1109 **Figure S9. Differentially expressed genes in Cas13bt3-VEGFA against Cas13bt3-NT.**
1110 Volcano plots from scRNA-seq for each retinal cell type showing differentially expressed
1111 genes between retinal organoid infected with Cas13bt3-VEGFA sgRNA and Cas13bt3-NT
1112 sgRNA. Significant downregulation of VEGFA in RPE cells is highlighted in red.

1113

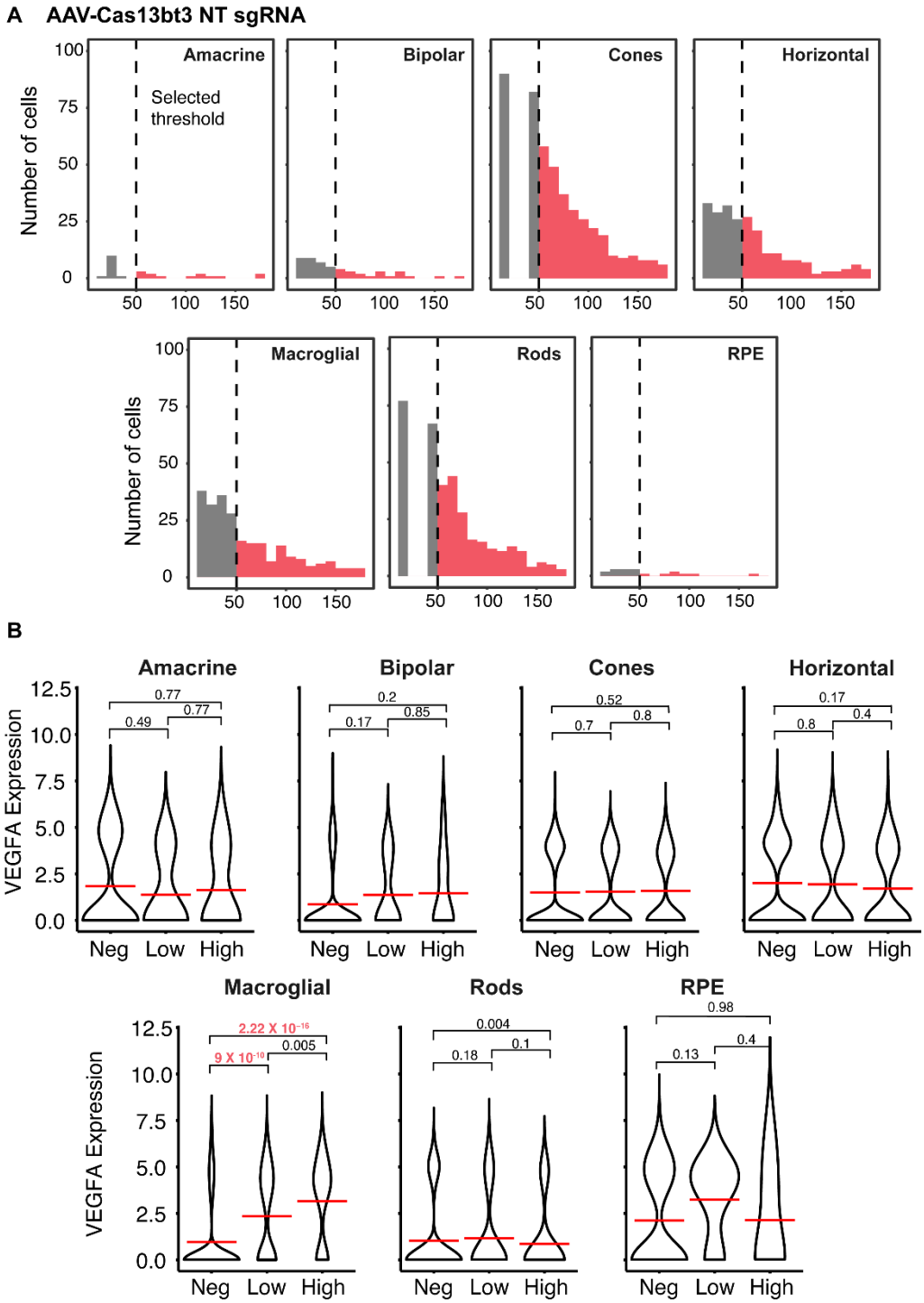
A AAV-Cas13bt3 NT sgRNA
Amacrine
Bipolar
Cones
Horizontal
Selected threshold
Number of cells
Macroglial
Rods
RPE
B
VEGFA Expression
Neg
Low
High
0.77
0.77
0.49
0.2
0.17
0.85
0.52
0.7
0.8
0.17
0.8
0.4
2.22 X 10⁻¹⁶
9 X 10⁻¹⁰
0.005
0.004
0.18
0.1
0.98
0.13
0.4

1114

1115 **Figure S10. Cas13bt3-NT sgRNA treatment in retinal organoids. (A)** Expression of
1116 Cas13bt3 by number of reads across retinal cell types in NT sgRNA treatment group. **(B)** Violin
1117 plots of VEGFA expression in cells with low and high expression of Cas13bt3 against
1118 Cas13bt3 negative cells showed no significant differences.

1119

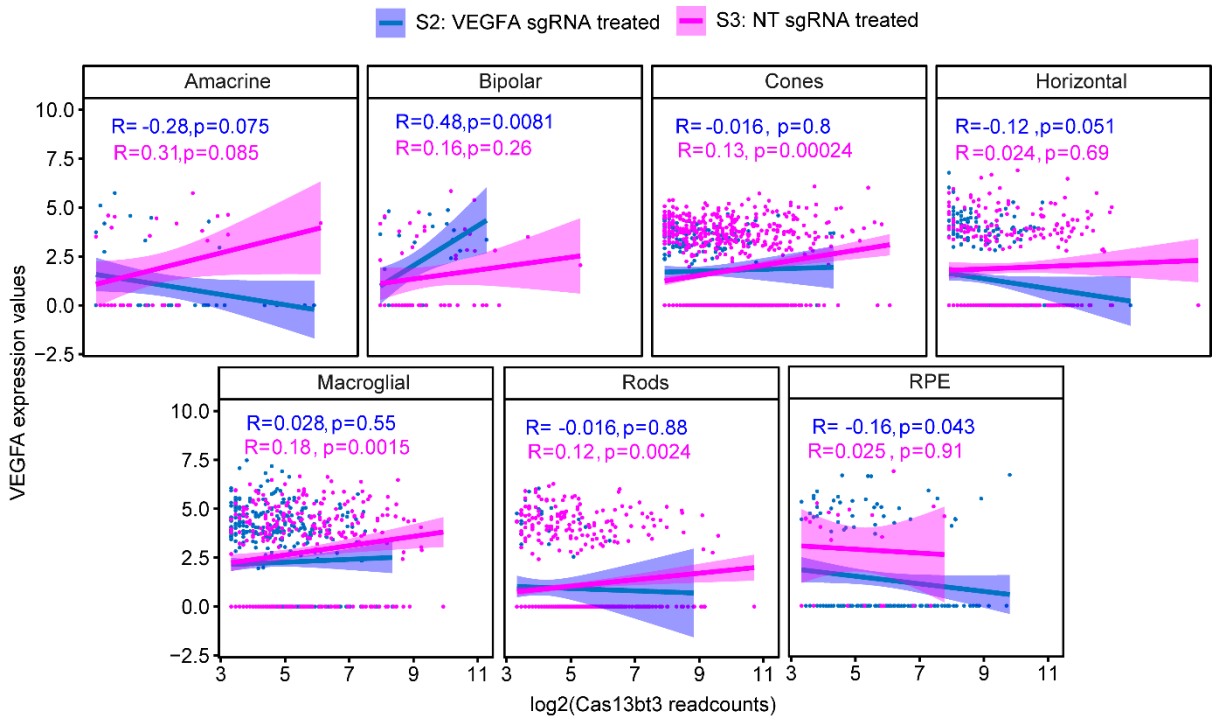
S2: VEGFA sgRNA treated
S3: NT sgRNA treated
Amacrine
R= -0.28,p=0.075
R=0.31,p=0.085
Bipolar
R=0.48,p=0.0081
R=0.16,p=0.26
Cones
R= -0.016, p=0.8
R=0.13, p=0.00024
Horizontal
R=-0.12 ,p=0.051
R=0.024, p=0.69
Macroglial
R=0.028, p=0.55
R=0.18, p=0.0015
Rods
R= -0.016, p=0.88
R=0.12, p=0.0024
RPE
R= -0.16, p=0.043
R=0.025, p=0.91
VEGFA expression values
10.0
7.5
5.0
2.5
0.0
−2.5
3
5
7
9
11
log2(Cas13bt3 readcounts)

1120

1121 **Figure S11. Expression of Cas13bt3 plotted against expression of VEGFA mRNA across**
1122 **cell types in NT sgRNA and VEGFA sgRNA groups.**

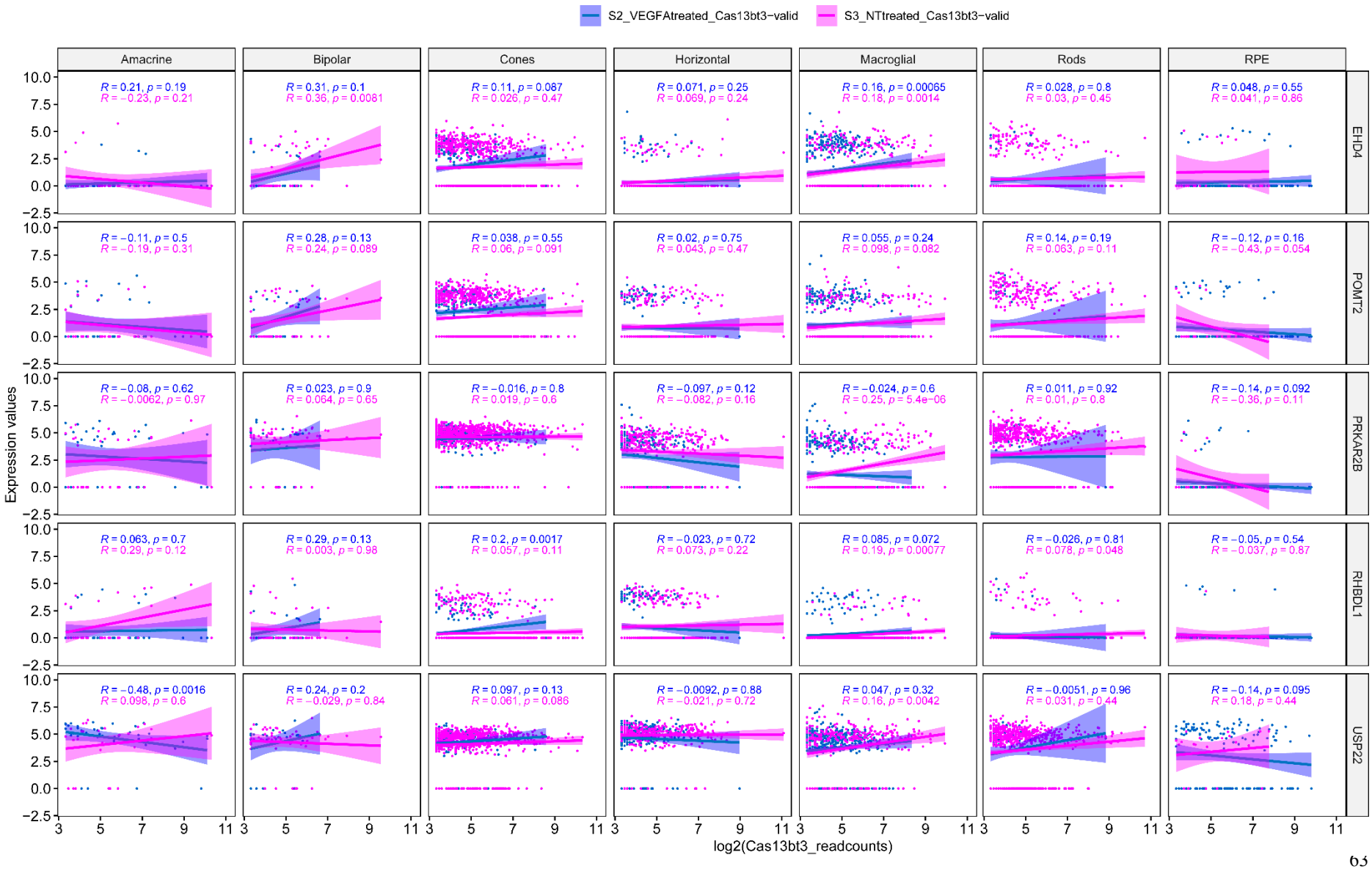
S2_VEGFAtreated_Cas13bt3−valid
S3_NTtreated_Cas13bt3−valid
Amacrine
Bipolar
Cones
Horizontal
Macroglial
Rods
RPE
EHD4
POMT2
PRKAR2B
RHBDL1
USP22
R = 0.21, p = 0.19
R = −0.23, p = 0.21
R = 0.31, p = 0.1
R = 0.36, p = 0.0081
R = 0.11, p = 0.087
R = 0.026, p = 0.47
R = 0.071, p = 0.25
R = 0.069, p = 0.24
R = 0.16, p = 0.00065
R = 0.18, p = 0.0014
R = 0.028, p = 0.8
R = 0.03, p = 0.45
R = 0.048, p = 0.55
R = 0.041, p = 0.86
R = −0.11, p = 0.5
R = −0.19, p = 0.31
R = 0.28, p = 0.13
R = 0.24, p = 0.089
R = 0.038, p = 0.55
R = 0.06, p = 0.091
R = 0.02, p = 0.75
R = 0.043, p = 0.47
R = 0.055, p = 0.24
R = 0.098, p = 0.082
R = 0.14, p = 0.19
R = 0.063, p = 0.11
R = −0.12, p = 0.16
R = −0.43, p = 0.054
R = −0.08, p = 0.62
R = −0.0062, p = 0.97
R = 0.023, p = 0.9
R = 0.064, p = 0.65
R = −0.016, p = 0.8
R = 0.019, p = 0.6
R = −0.097, p = 0.12
R = −0.082, p = 0.16
R = −0.024, p = 0.6
R = 0.25, p = 5.4e−06
R = 0.011, p = 0.92
R = 0.01, p = 0.8
R = −0.14, p = 0.092
R = −0.36, p = 0.11
R = 0.063, p = 0.7
R = 0.29, p = 0.12
R = 0.29, p = 0.13
R = 0.003, p = 0.98
R = 0.2, p = 0.0017
R = 0.057, p = 0.11
R = −0.023, p = 0.72
R = 0.073, p = 0.22
R = 0.085, p = 0.072
R = 0.19, p = 0.00077
R = −0.026, p = 0.81
R = 0.078, p = 0.048
R = −0.05, p = 0.54
R = −0.037, p = 0.87
R = −0.48, p = 0.0016
R = 0.098, p = 0.6
R = 0.24, p = 0.2
R = −0.029, p = 0.84
R = 0.097, p = 0.13
R = 0.061, p = 0.086
R = −0.0092, p = 0.88
R = −0.021, p = 0.72
R = 0.047, p = 0.32
R = 0.16, p = 0.0042
R = −0.0051, p = 0.96
R = 0.031, p = 0.44
R = −0.14, p = 0.095
R = 0.18, p = 0.44
Expression values
log2(Cas13bt3_readcounts)

1123

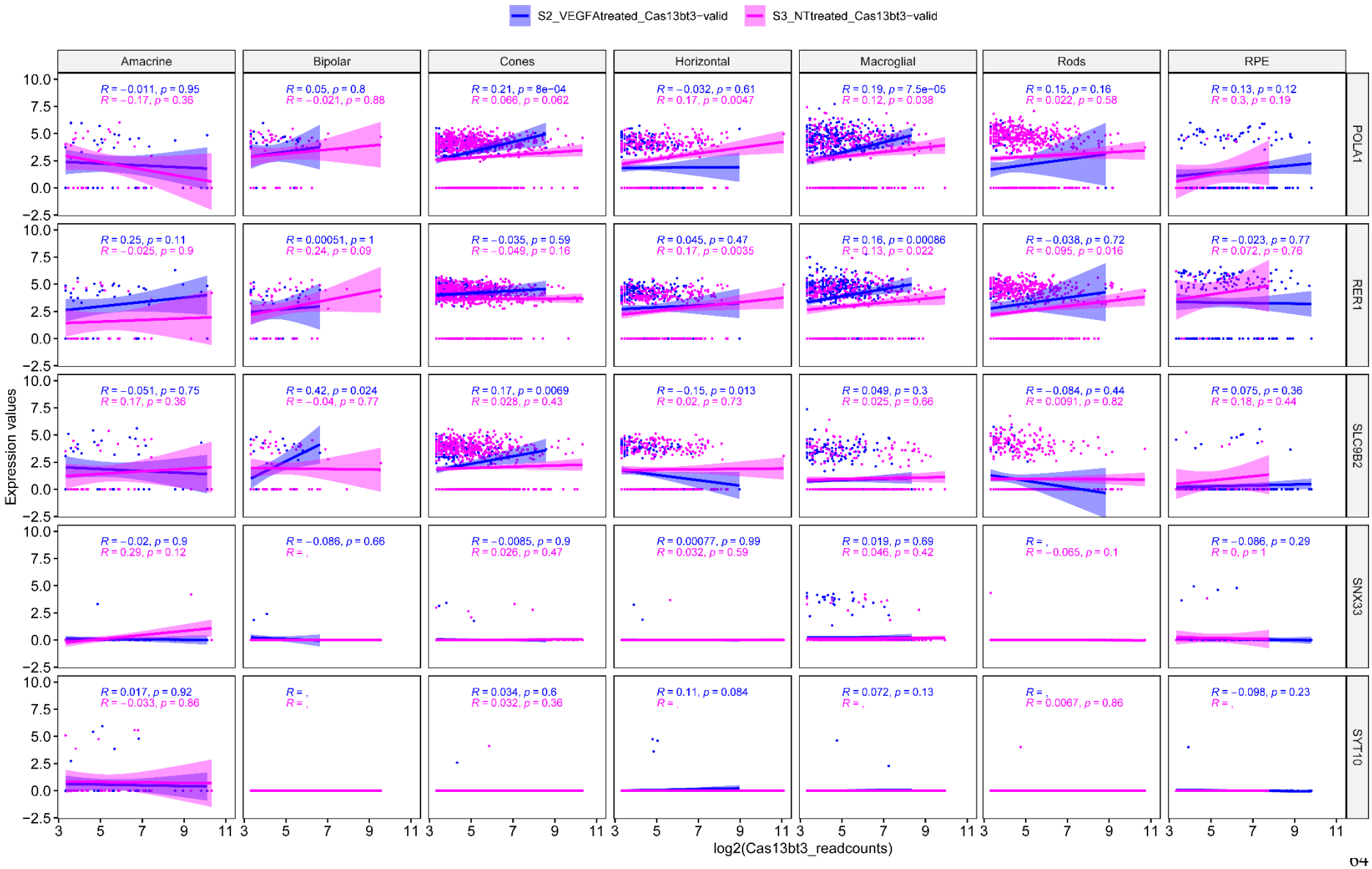
S2_VEGFAtreated_Cas13bt3−valid
S3_NTtreated_Cas13bt3−valid
Amacrine
Bipolar
Cones
Horizontal
Macroglial
Rods
RPE
POLA1
RER1
SLC9B2
SNX33
SYT10
Expression values
log2(Cas13bt3_readcounts)
R = −0.011, p = 0.95
R = −0.17, p = 0.36
R = 0.05, p = 0.8
R = −0.021, p = 0.88
R = 0.21, p = 8e−04
R = 0.066, p = 0.062
R = −0.032, p = 0.61
R = 0.17, p = 0.0047
R = 0.19, p = 7.5e−05
R = 0.12, p = 0.038
R = 0.15, p = 0.16
R = 0.022, p = 0.58
R = 0.13, p = 0.12
R = 0.3, p = 0.19
R = 0.25, p = 0.11
R = −0.025, p = 0.9
R = 0.00051, p = 1
R = 0.24, p = 0.09
R = −0.035, p = 0.59
R = −0.049, p = 0.16
R = 0.045, p = 0.47
R = 0.17, p = 0.0035
R = 0.16, p = 0.00086
R = 0.13, p = 0.022
R = −0.038, p = 0.72
R = 0.095, p = 0.016
R = −0.023, p = 0.77
R = 0.072, p = 0.76
R = −0.051, p = 0.75
R = 0.17, p = 0.36
R = 0.42, p = 0.024
R = −0.04, p = 0.77
R = 0.17, p = 0.0069
R = 0.028, p = 0.43
R = −0.15, p = 0.013
R = 0.02, p = 0.73
R = 0.049, p = 0.3
R = 0.025, p = 0.66
R = −0.084, p = 0.44
R = 0.0091, p = 0.82
R = 0.075, p = 0.36
R = 0.18, p = 0.44
R = −0.02, p = 0.9
R = 0.29, p = 0.12
R = −0.086, p = 0.66
R = ,
R = −0.0085, p = 0.9
R = 0.026, p = 0.47
R = 0.00077, p = 0.99
R = 0.032, p = 0.59
R = 0.019, p = 0.69
R = 0.046, p = 0.42
R = ,
R = −0.065, p = 0.1
R = −0.086, p = 0.29
R = 0, p = 1
R = 0.017, p = 0.92
R = −0.033, p = 0.86
R = ,
R = ,
R = 0.034, p = 0.6
R = 0.032, p = 0.36
R = 0.11, p = 0.084
R = ,
R = 0.072, p = 0.13
R = ,
R = ,
R = 0.0067, p = 0.86
R = −0.098, p = 0.23
R = ,

1124

1125 **Figure S12. Correlation plots of Cas13bt3 with VEGFA expression in the various retinal cell types for the predicted off-target genes of**
1126 **VEGFA sgRNA.**

1127

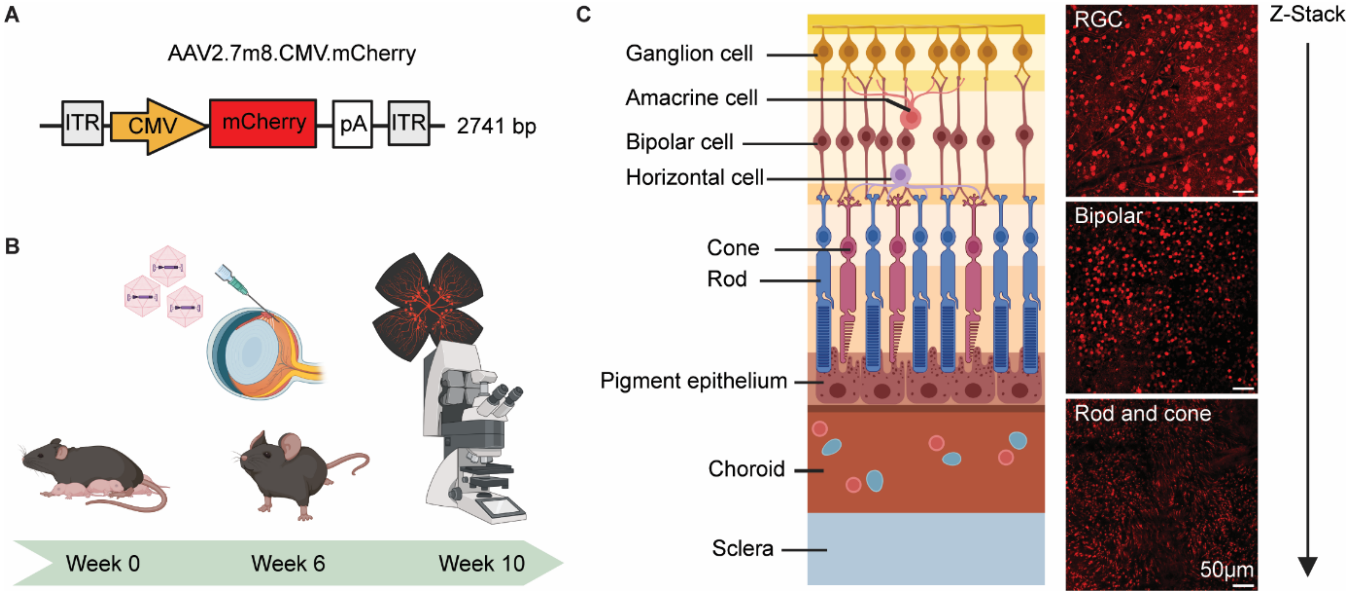
A
AAV2.7m8.CMV.mCherry
ITR
CMV
mCherry
pA
ITR
2741 bp
B
Week 0
Week 6
Week 10
C
Ganglion cell
Amacrine cell
Bipolar cell
Horizontal cell
Cone
Rod
Pigment epithelium
Choroid
Sclera
RGC
Bipolar
Rod and cone
50μm
Z-Stack

1128 **Figure S13. Intravitreal delivery of AAV2.7m8 achieves strong transduction of mice**
1129 **photoreceptors. (A)** Schematic of AAV2.7m8 virus carrying mCherry reporter. **(B)** Schematic
1130 of experimental procedure for intravitreal injection of C57J/BL6 mice eyes. **(C)** Confocal
1131 microscope images of retinal flatmount 4 weeks post intravitreal injection, showing
1132 transduction of ganglion, bipolar, cone and rod cells with reference image of retinal cell layers.

1133

1134

1135

1136

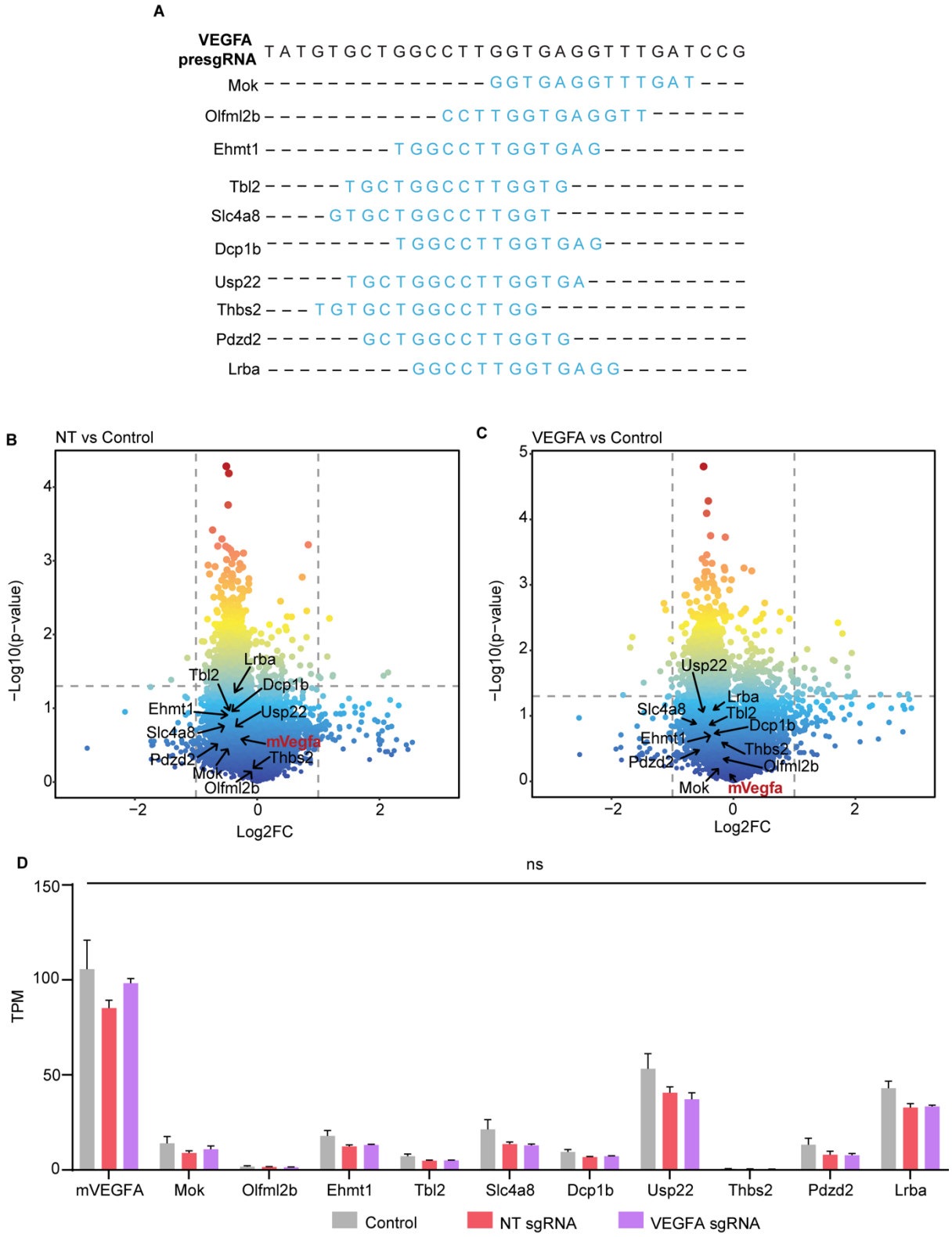
A
VEGFA presgRNA TATGTGCTGGCCTTGGTGAGGTTTGATCCG
Mok ----------GGTGAGGTTTGAT---
Olfml2b ----------CCTTGGTGAGGTT------
Ehmt1 --------TGGCCTTGGTGAG---------
Tbl2 -----TGCTGGCCTTGGTG----------
Slc4a8 ----GTGCTGGCCTTGGT----------
Dcp1b --------TGGCCTTGGTGAG---------
Usp22 -----TGCTGGCCTTGGTGA----------
Thbs2 ---TGTGCTGGCCTTGG----------
Pdzd2 ------GCTGGCCTTGGTG----------
Lrba ---------GGCCTTGGTGAGG--------
B
NT vs Control
−Log10(p−value)
Log2FC
Lrba
Tbl2
Dcp1b
Ehmt1
Usp22
Slc4a8
mVegfa
Pdzd2
Thbs2
Mok
Olfml2b
C
VEGFA vs Control
−Log10(p−value)
Log2FC
Usp22
Lrba
Slc4a8
Tbl2
Dcp1b
Ehmt1
Thbs2
Pdzd2
Olfml2b
Mok
mVegfa
D
ns
TPM
mVEGFA
Mok
Olfml2b
Ehmt1
Tbl2
Slc4a8
Dcp1b
Usp22
Thbs2
Pdzd2
Lrba
Control
NT sgRNA
VEGFA sgRNA

1137

1138 **Figure S14. Cas13bt3 off-target effects in Kimba mice. (A)** Schematic of candidate off-
1139 target genes to VEGFA sgRNA in mouse transcriptome. Volcano plots of differentially
1140 expressed genes from Kimba mice retinas treated with AAV2.7m8 carrying **(B)** Cas13bt3-
1141 NTsgRNA and **(C)** Cas13bt3-VEGFAsgRNA compared to vector controls. **(D)** Expression in
1142 TPM of mouse VEGFA and candidate off-target genes from RNA-seq.

1143

1144

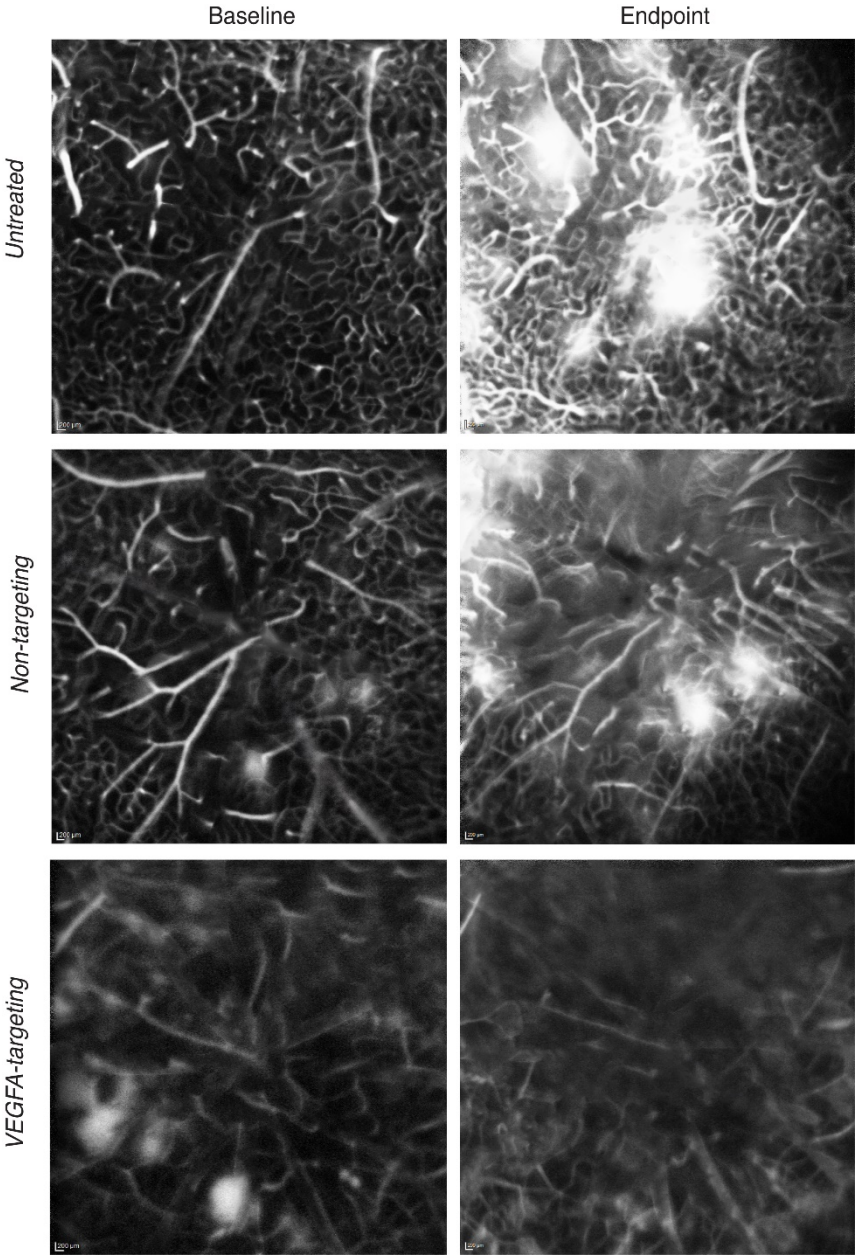
Baseline
Endpoint
Untreated
Non-targeting
VEGFA-targeting

1145

1146 **Figure S15. Original fundus fluorescein angiography images from Kimba mice retinae.**

1147

1148

1149

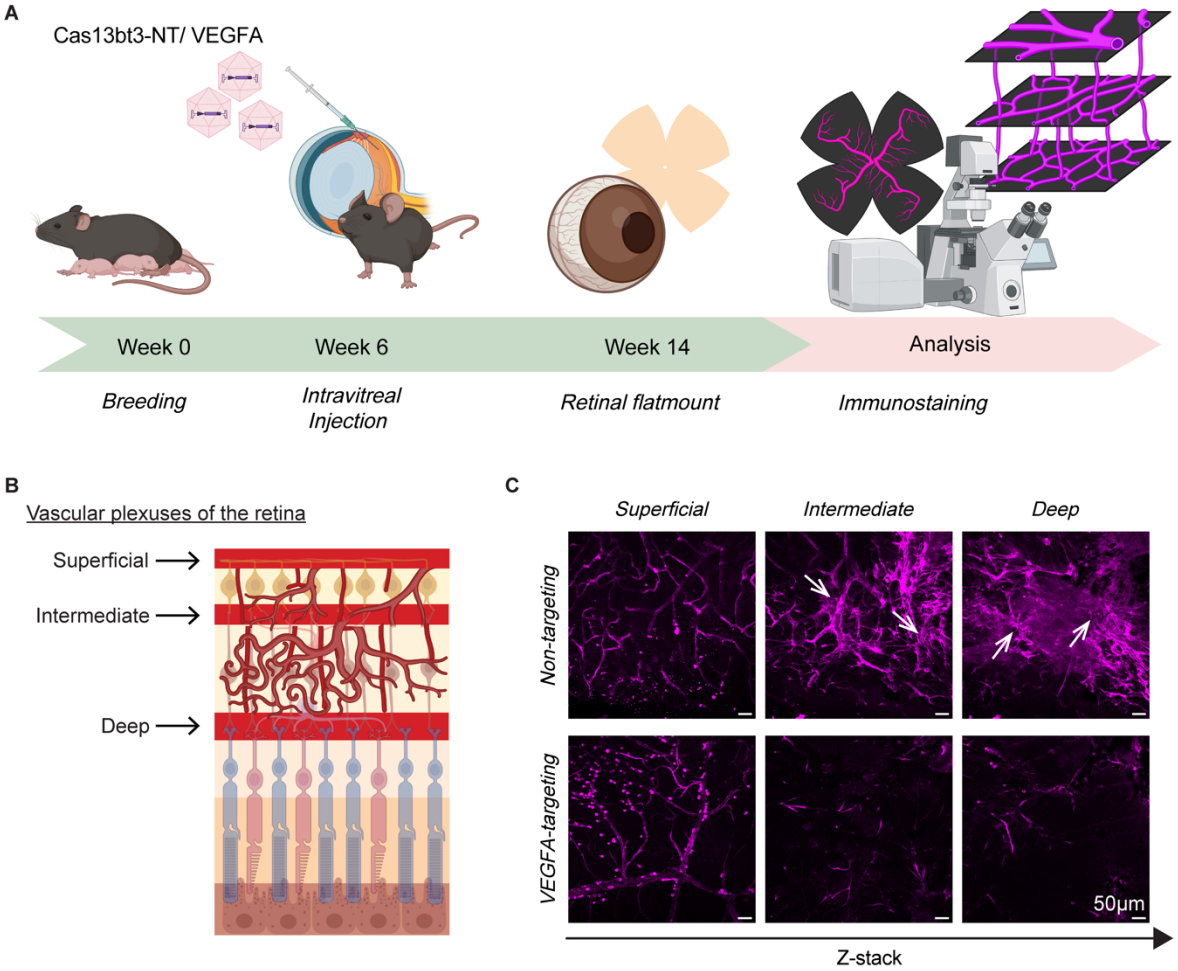
A
Cas13bt3-NT/ VEGFA
Week 0
Week 6
Week 14
Analysis
Breeding
Intravitreal Injection
Retinal flatmount
Immunostaining
B
Vascular plexuses of the retina
Superficial
Intermediate
Deep
C
Superficial
Intermediate
Deep
Non-targeting
VEGFA-targeting
50µm
Z-stack

1150

1151 **Figure S16. Imaging of retinal vascular plexuses Kimba mice treated with Cas13bt3-**
1152 **NTsgRNA and Cas13bt3-VEGFAsgRNA. (A)** Schematic of experimental procedure for
1153 imaging retinal vascular plexuses. **(B)** Schematic of the different retinal plexuses. **(C)** Confocal
1154 imaging of the retinal plexuses, 8 weeks after Cas13bt3 treatment, immunolabelled with
1155 laminin. Magnification 40X, scale bar: 50µm. White arrows indicate leaky vessel structure.

1156

1157

1158

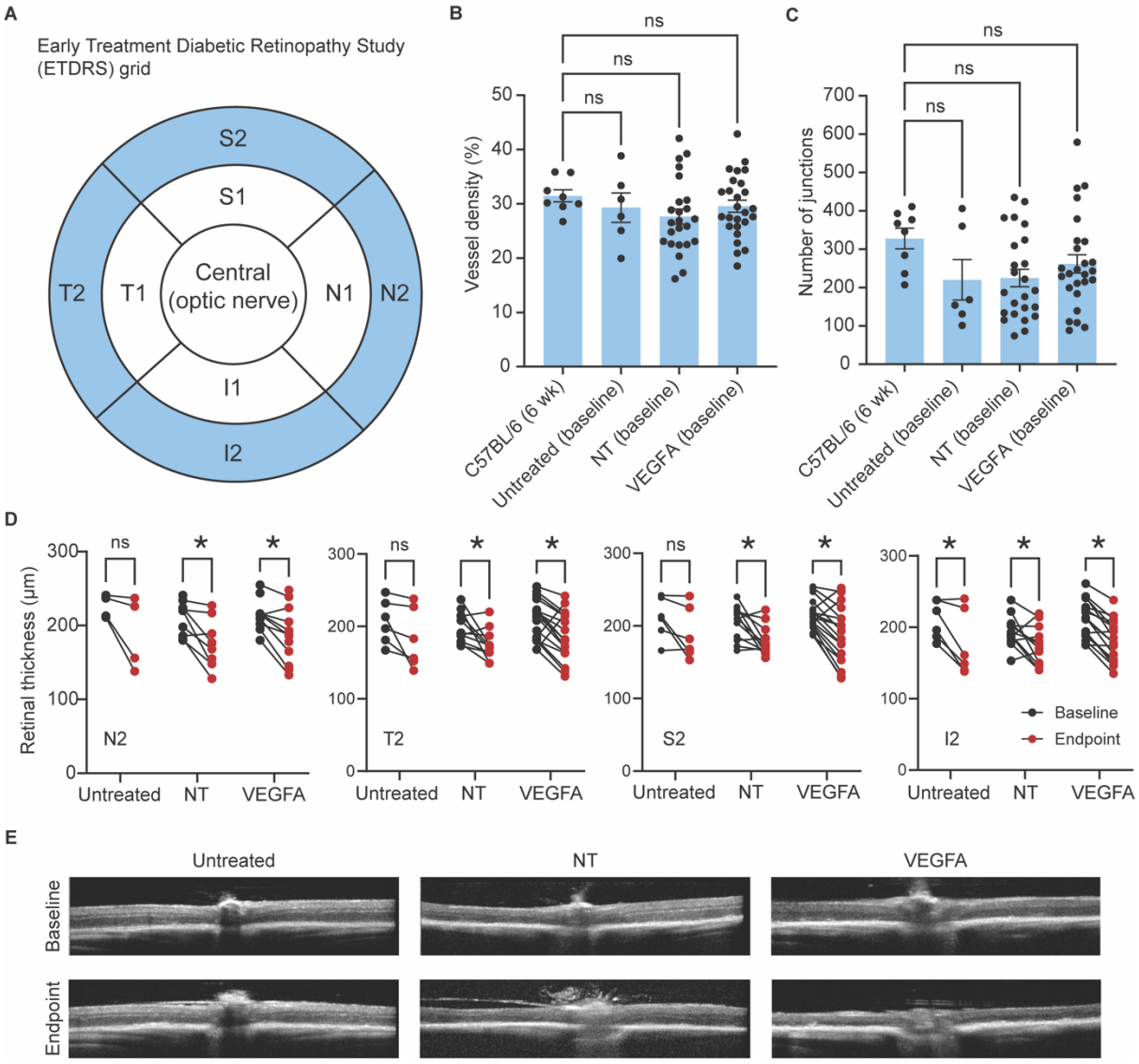
A
Early Treatment Diabetic Retinopathy Study
(ETDRS) grid
S2
S1
T2
T1
Central
(optic nerve)
N1
N2
I1
I2
B
Vessel density (%)
ns
ns
ns
C57BL/6 (6 wk)
Untreated (baseline)
NT (baseline)
VEGFA (baseline)
C
Number of junctions
ns
ns
ns
C57BL/6 (6 wk)
Untreated (baseline)
NT (baseline)
VEGFA (baseline)
D
Retinal thickness (µm)
N2
T2
S2
I2
Untreated
NT
VEGFA
Baseline
Endpoint
E
Untreated
NT
VEGFA
Baseline
Endpoint

1159

1160 **Figure S17. Retinal thickness readings from optical coherence tomography (OCT) in**
1161 **Kimba mice. (A)** Early Treatment of Diabetic Retinopathy Study (ETDRS) grid showing
1162 segments of the retina analysed using OCT. C:Central (optic nerve); N1: Inner nasal; N2: Outer
1163 Nasal; T1: Inner temporal; T2: Outer temporal; S1: inner superior; S2: Outer superior; I1: Inner
1164 inferior; I2: Outer inferior. **(B)** Vessel density and **(C)** number of junctions readings from FFA
1165 images of Kimba mice at baseline compared to wildtype (C57BL/6) mice. **(D)** Plot of
1166 difference in total retinal thickness in untreated and treated Kimba mice between baseline and
1167 endpoint. **(E)** Representative OCT images from untreated and treated Kimba mice at endpoint.

1168

1169

Reagent or Resource	Source	Identifier
Chemicals		
DMEM	Thermo Fisher Scientific	Cat# 11965092
DMEM/F12	Thermo Fisher Scientific	Cat# 11320033
Opti-MEM	Thermo Fisher Scientific	Cat# 31985070
TrypLE™ Express	Thermo Fisher Scientific	Cat# 12605093
GlutaMAX™ Supplement	Thermo Fisher Scientific	Cat# 35050061
FBS	Bovogen Biologicals	SFBS-AU
Antibiotic-Antimycotic	Thermo Fisher Scientific	Cat# 15240062
DPBS	Thermo Fisher Scientific	Cat# 14190250
Lipofectamine™ 3000 Transfection Reagent	Thermo Fisher Scientific	Cat# L3000001
ViaFect™ Transfection Reagent	Promega Corporation	Cat# E4982
NEB® Stable Competent E. coli, High Efficiency	New England Biolabs	Cat# C3040I
rCutSmart™ Buffer	New England Biolabs	Cat# B6004S
NEB® 10-beta/Stable Outgrowth Medium	New England Biolabs	Cat# B9035S
NucBlue™ Live ReadyProbes™ Reagent (Hoechst 33342)	Thermo Fisher Scientific	Cat# R37605
LB (Lennox L) agar	Thermo Fisher Scientific	Cat# 22700025
2-YT Broth	Thermo Fisher Scientific	Cat# 22712020
Carbenicillin Disodium Salt	Thermo Fisher Scientific	Cat# 10177012
GelRed® nucleic acid gel stain	Biotium	Cat# 41003
Phosphate buffered saline	Merck	Cat# P3813
Tween-20	Merck	Cat# P1379
Triton-X-100	Amresco	Cat# 0694
RIPA Lysis and Extraction Buffer	Thermo Fisher Scientific	Cat# 89900

Pierce™ Phosphatase Inhibitor Mini Tablets	Thermo Fisher Scientific	Cat# A32957
NuPAGE™ MES SDS Running Buffer (20X)	Thermo Fisher Scientific	Cat# NP0002
NuPAGE™ LDS Sample Buffer (4X)	Thermo Fisher Scientific	Cat# NP0007
0.5% Proxymethacaine hydrochloride (Alcaine™)	Alcon	N/A
0.5% Tropicamide (Mydriacyl)	Alcon	N/A
GenTeal™ Gel	Alcon	N/A
Ketamine, 100 mg/mL	Troy Laboratories	Ketamil
Xylazine, 100 mg/mL	Troy Laboratories	Ilium Xylazil-100
Experimental models: Cell lines		
Human: HEK293FT	Thermo Fisher Scientific	R70007
Human: ARPE-19	ATCC	CRL-2302™
Human: Müller 1 (MIO-M1)	UCL Institute of Ophthalmology, London	(*63*)
Experimental models: Organisms/ strains		
Human: 3D retinal organoid	Children's Medical Research Institute	(*27*)
Kimba Mouse	The University of Western Australia	(*29*)
Antibodies		
Mouse anti-actin, clone C4	Merck	MAB1501
Rabbit anti-HA, C29F4	Cell Signaling Technology	#3724
Mouse anti-rhodopsin, 1D4	Abcam	ab5417
Rat mCherry monoclonal 16D7, Alexa Fluor™ 594	Thermo Fisher Scientific	Cat# M11240
Rat anti-laminin monoclonal, α-2 chain	Merck	L0663
Donkey anti-rat AffiniPure Fragment IgG (H + L), Alexa Fluor™ 647	Jackson ImmunoResearch	712-606-150

Donkey mouse AffiniPure Fragment IgG (H + L), Alexa Fluor™	Jackson ImmunoResearch	715-546-151
Goat anti-rabbit IgG (H+L) Secondary Antibody, HRP	Thermo Fisher Scientific	Cat# 31460
Goat anti-Mouse IgG (H+L) Secondary Antibody, HRP	Thermo Fisher Scientific	Cat# 62-6520
Anti-Arrestin C antibody, C-terminal	Abcam	189437
Monoclonal Anti-Opsin antibody produced in mouse	Merck	O4886
Sheep anti Human chx 10 (Visual system homeobox 2) (NT)	ExAlpha	XII80P
CRALBP Monoclonal Antibody (B2)	Thermo Fisher Scientific	MA1-813
Anti-Prox 1 Antibody	Merck	AB5475
HuC/HuD Monoclonal Antibody (16A11)	Thermo Fisher Scientific	A21271
Commercial kits		
RNeasy Mini kit	Qiagen	Cat# 74106
Monarch® Total RNA Miniprep Kit	New England Biolabs	Cat# T2010S
High-Capacity cDNA Reverse Transcription Kit	Thermo Fisher Scientific	Cat# 4368814
Q5® Hot Start High-Fidelity Master Mix	New England Biolabs	Cat# M0494S
TaqMan™ Fast Advanced Master Mix	Thermo Fisher Scientific	Cat# 4444557
SYBR™ Green PCR Master Mix	Thermo Fisher Scientific	Cat# 4309155
Human VEGF DuoSet ELISA	R & D systems	Cat# DY293B
Recombinant DNA		
pAAV.CMV-CasRx mCh	Addgene	203442
pAAV.CMV-CasRx-VEGFA sgRNA	Addgene	203443
pAAV.CMV-CasRx-VEGFA sgRNA array	Addgene	203444
pAAV.CMV-Cas13bt3-NT sgRNA	Addgene	203446

pAAV.CMV-Cas13bt3-VEGFA sgRNA	Addgene	203447
pAAV.CMV-Cas13bt3-VEGFA sgRNA array	Addgene	203448
pAAV.CMV-Cas13bt3 (GenScript CO)-NT sgRNA	Addgene	203451
pAAV.CMV-Cas13bt3 (GenScript CO)-VEGFA sgRNA	Addgene	203452
Software and algorithms		
GraphPad Prism 10	GraphPad	https://www.graphpad.com/scientific-software/prism/E/
Benchling	Benchling	https://www.benchling.com/
Fiji-ImageJ	National Institutes of Health	https://imagej.net/software/fiji/
GenSmart™ Codon Optimisation	GenScript	https://www.genscript.com/gensmart-free-gene-codon-optimization.html
IDT Codon Optimisation Tool	Integrated DNA Technologies	https://sg.idtdna.com/pages/tools/codon-optimization-tool
STAR (2.7.11a)	(*55*)	https://github.com/alexdobin/STAR
DESeq2 (v3.18)	(*64*)	https://bioconductor.org/packages/release/bioc/html/DESeq2.html
Seurat (v5)	(*65*)	https://satijalab.org/seurat/
Cell Ranger (v7.2)	10X Genomics	https://www.10xgenomics.com/support/software/cell-ranger
ImageLab (v6.1)	Bio-Rad	https://www.bio-rad.com/en-au/product/image-lab-software
R (v4.3.2)	R Core Team	https://cran.r-project.org/
RStudio (v2023.09.1)	Posit PBC	https://posit.co/download/rstudio-desktop/

Adobe Photoshop (v25)	Adobe Inc.	https://www.adobe.com/au/products/photoshop.html
AngioTool (v0.5)	National Cancer Institute	https://ccrod.cancer.gov/confluence/display/ROB2/Downloads
Equipment		
HRA + OCT Spectralis	Heidelberg Engineering	N/A
Leica Stellaris 5 confocal microscope	Leica Microsystems	N/A

1170

1171 **Table S1.**

1172 Key resources.

1173

Quantitative PCR		
Name	**Source**	**Identifier**
Human VEGFA (Hs00900055_m1)	Thermo Fisher Scientific	Cat# 4331182
Mouse VEGFA (Mm00437306_m1)	Thermo Fisher Scientific	Cat# 4331182
Human GAPDH (Hs02786624_g1)	Thermo Fisher Scientific	Cat# 4448489
Mouse GAPDH (Mm99999915_g1)	Thermo Fisher Scientific	Cat# 4448489
Standard PCR		
Name	**Sequence (5' - 3')**	**Source**
Cas13bt3_FWD	CGGCGAACAGGGTGATAAA	Integrated DNA Technologies
Cas13bt3_REV	CTGTGCTGGGCTTCAAGATA	Integrated DNA Technologies

1174

1175 **Table S2.**

1176 Primers used in this study.

1177

1178

1179